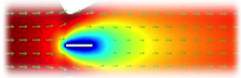
Fenómenos de Transporte

Revista Mexicana de Ingeniería Química
Vol. 13, No. 1 (2014) 237-257

UPSCALED MODEL FOR DISPERSIVE MASS TRANSFER IN A TUBULAR POROUS MEMBRANE SEPARATOR

MODELO ESCALADO PARA LA TRANSFERENCIA DISPERSIVA DE MASA EN UN SEPARADOR TUBULAR POR MEMBRANA POROSA

F.J. Valdés-Parada[1], J.A. Ochoa-Tapia[1], E. Salinas-Rodríguez[1*], S. Gómez-Torres[1] and M.G. Hernández[2]

[1]*Departamento de Ingeniería de Procesos e Hidráulica, Universidad Autónoma Metropolitana-Iztapalapa, Av. San Rafael Atlixco 186 col. Vicentina, C.P. 09340, México D.F., México.*
[2]*Departamento de Ciencias Básicas, Área de FAMA, Universidad Autónoma Metropolitana-Azcapotzalco*

Received November 22, 2013; Accepted January 25, 2014

Abstract

In this work, the steady-state mass transfer of a non-reactive species in a tubular separator involving a porous membrane is studied. This type of equipment has received considerable attention in the literature since it can be used for gas-gas separation processes. In specific, in this work we are interested in studying transport of oxygen from an air current to a pure helium flow. The air is transported in the annular region, whereas the helium is flowing in countercurrent within the inner compartment of the system. The membrane is permeable to gases in different proportions; however, only oxygen is assumed to constitute a dilute solution in both regions of the system. To derive the mathematical model, we averaged the pointwise equations in the system cross-section generating a system of two ordinary differential equations representing non-equilibrium mass transfer in each region of the system. These upscaled equations are written in terms of effective-medium coefficients that capture the essential features from the pointwise transport and are predicted from the solution of the associated closure problem. To evaluate the predictive capabilities of the model, we compared the concentration profiles with those from solving the pointwise equations. The influence of the membrane permeability to oxygen transfer is studied and we found a close correspondence between the pointwise and upscaled models.

Keywords: mass transfer, tubular membrane separator, oxygen transfer, non-equilibrium model, upscaling.

Resumen

En este trabajo, se estudia la tranferencia de masa en estado estacionario de una especie no reactiva en un separador tubular que involucra una membrana porosa. Este tipo de equipo ha recibido considerable atención en la literatura ya que puede usarse en procesos de separación gas-gas. En específico, en este trabajo estamos interesados en estudiar el transporte de oxígeno de una corriente de aire hacia un flujo de helio puro. El aire es transportado en la región anular, mientras que el helio fluye a contracorriente en el compartimiento interno del sistema. La membrana es permeable a los gases en diferentes proporciones; sin embargo, se supone que sólo el oxígeno forma una solución diluida en ambas regiones del sistema. Para desarrollar el modelo matemático, se promediaron las ecuaciones puntuales en la sección transversal del sistema, lo que da lugar a un sistema de dos ecuaciones diferenciales ordinarias representando la transferencia de masa de no equilibrio en cada región del sistema. Estas ecuaciones escaladas están escritas en términos de coeficientes de medio efectivo que capturan las características esenciales del transporte puntual y se predicen a partir de la solución del problema de cerradura asociado. Para evaluar las capacidades predictivas del modelo, se compararon los perfiles de concentración con los que resultan de resolver las ecuaciones puntuales. Se estudió la influencia de la permeabilidad de membrana sobre la transferencia de oxígeno y encontramos una cercana correspondencia entre los modelos puntual y escalado.

Palabras clave: transferencia de masa, separador tubular de membrana, transferencia de oxígeno, modelo de no equilibrio, escalamiento.

[*]*Corresponding author. E-mail*: sabe@xanum.uam.mx

1 Introduction

Membrane separation processes have significantly progressed during the past two decades and have reached a development level that has allowed studying both industrial-scale and nano-scale systems (Faucheux, 2008; Rebollar-Perez *et al*., 2010). According to Coronas and Santamaría (1999), most membrane applications can be classified in three groups: as an *extractor*, as a *distributor* or as a *contactor*. In these cases the membrane can be used for separation purposes and to carry out catalytic reactions.

Due to its molecular sieving effect, zeolite membranes are able to discriminate between the components of liquid or gas mixtures (Bowen *et al*., 2004; McLeary *et al*., 2006; Freeman *et al*., 2008; Gascon *et al*., 2012). Among several applications of membranes (Hernández *et al*., 2012), their use in gas-phase separation processes has received considerable interest during the last years. In particular, pure oxygen has been regarded as a high economically and environmentally safe feedstock for the steel and cement industries and also for the gasification of coal in oxy-fuel power plants, among other applications (Wang *et al*., 2004; Jiang *et al*., 2011). Nevertheless, the production of essentially pure oxygen is very difficult since some nitrogen always permeates with the oxygen through the membrane (Zhu *et al*., 2008; Liang *et al*., 2010). Therefore, a proper description of the gases diffusion within the pores is needed to understand this process. To carry out the separation of oxygen from the gas current, a shell-and-tube permeator (Fig. 1), has been suggested in the literature with promising efficiencies (Li *et al*., 2000; Wang *et al*., 2003, 2004).

Concerning mathematical modeling of tubular membranes, Wang *et al*. (2004) reported a model to simulate the isothermal steady-state air separation process in a membrane permeator using helium as carrier gas. These authors neglected the helium permeation and assumed laminar flow. With these assumptions they obtained a local differential equation for the oxygen flow rate, an overall and an oxygen material balance equations. These equations were solved numerically using the Gear method. They obtained the dependence of oxygen permeation flux on the air and on the helium flow rates at different temperatures and compared their numerical results with their experimental results obtaining good agreement. Their model also allowed them to predict the local O_2 permeation flow rate.

Another approach is the use of molecular dynamics to understand the behavior of tubular membranes. For example, Abdel-Jawad *et al*. (2007) report a computational fluid dynamic approach to integrate diffusion through a molecular sieve silica membrane described by the Stefan-Maxwell model. Continuum gas flows were described by the Navier-Stokes equations in 2D at steady state. They found that the partial pressure axial distributions were constant in the feed /retentate and the permeated streams. Besides, the radial variation of axial velocity across the flow was practically the same for all axial positions at the permeate stream. They also found a linear behavior of the axial velocity with the axial coordinate.

In this work, we present a different approach based on the hierarchical nature (Cushman, 1997) of the tubular membrane permeator (Fig. 1). In this case, there are two types of transport phenomena taking place, one at the macroscale (at permeator scale) and another at the microscale (at the cross-section). As matter of fact, many transport processes of hierarchical nature are driven by transport phenomena taking place at the interfaces as explained by Whitaker (2009). The coupling between transport phenomena at the microscale and at the macroscale suggests that the governing equations at the macroscale can be derived by properly averaging their microscale counterparts. In this work, the averaging process is based upon the volume averaging method (Whitaker, 1999) following an approach similar to that used by Wood (2009) and it basically consists on: 1) applying an averaging operator to the partial differential equations governing transport at the microscale; 2) expressing any remaining microscale quantity in terms of its average and spatial deviations; 3) deriving an expression for the spatial deviations in terms of average properties and 4) defining effective medium coefficients in terms of *filters* of the microscale information. Other works have been presented in the literature using similar upscaling approaches (Hussain, 2006; Kumar *et al*., 2013).

Since mass transport is taking place in the two portions of the system, two modeling approaches can arise for the macroscale description (see Chapter 2 in Whitaker, 1999). The first one is a model based on the assumption of local mass equilibrium and yields to a single differential equation for describing transport everywhere in the system. The second approach does not require such assumption and the macroscopic model consists of two coupled differential equations, one for each region of the system.

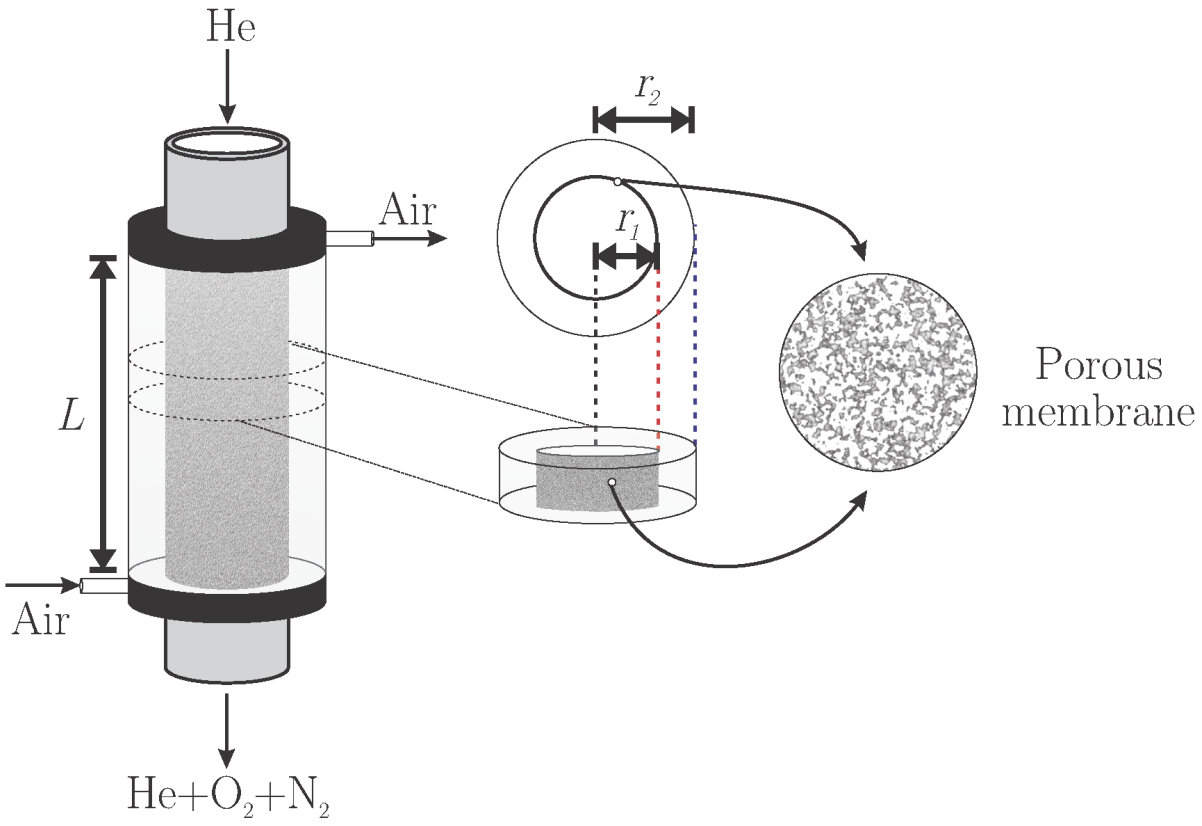

Fig. 1. Sketch of the tubular membrane permeator under consideration including the characteristic lengths of the system.

Despite the appealing simplicity of the equilibrium model, in this particular application it is not the best approach because the intrinsic phenomena taking place at the boundary do not appear explicitly in the model. In addition, both portions of the system are not in intimate contact. For this reason, in this work, we will derive a non-equilibrium upscaled model for the permeator sketched in Fig. 1 when used for oxygen separation using a zeolite porous membrane.

The paper is organized as follows: In Section 2 we provide the governing equations for mass and momentum transport at the microscale clearly stating our departing assumptions. Since one of them consists on regarding oxygen as a dilute solute in both regions, we use Fick's law as a constitutive expression for the mass flux, thus making it possible to solve the momentum transport equations independently from the mass transport expressions. In Section 3 we carry out the upscaling process for the mass transport equations that leads to the non-equilibrium model mentioned above. This section also includes a sensitivity analysis of the effective-medium coefficients involved in the model with the main independent dimensionless parameters. To test the predictive capabilities of the upscaled model, in Section 4 we compare the concentration profiles resulting from our approach with those resulting from solving the pointwise equations (*i.e.*, performing direct numerical simulations). Finally, we provide the corresponding conclusions along appendices with supplementary material regarding the closure process.

2 Microscale model

Let us consider a separation unit like the one sketched in Fig. 1. In the annular section, an air current is fed and the oxygen is selectively permeated through the membrane into the inner chamber where a carrier gas (usually a noble gas, like helium) is fed at counter-current. For the process under consideration, we adopt the following assumptions that will aid in stating the governing equations at the microscale:

1. Oxygen is sufficiently diluted in both sections

of the system so that Fick's law can be assumed applicable.

2. The characteristic length of the porous membrane (say ℓ) is such that it can be regarded as a boundary that separates the tube and the shell. This is acceptable as long as $\ell \ll r_1$.

3. Inertial momentum transport is assumed negligible with respect to viscous stress. This implies that the Reynolds number must be much less than the unity and laminar flow conditions prevail.

4. All fluids are assumed incompressible and Newtonian.

5. All fluid properties (*i.e.*, viscosity, density, molecular diffusivity) are constants.

6. The membrane permeability, P, is a known constant that can be obtained from experimental data.

7. Mass and momentum transport take place under steady-state and isothermal conditions.

8. The axial component of the velocity provides the most relevant contribution to momentum transport.

9. All transport processes are axi-symmetrical.

Under these circumstances, the pointwise governing equations for mass transfer of oxygen (species A), in their molar form, are

Region-I

$$v_{zI}\frac{\partial c_{AI}}{\partial z} = \frac{\mathscr{D}_{AI}}{r}\frac{\partial}{\partial r}\left(r\frac{\partial c_{AI}}{\partial r}\right) + \mathscr{D}_{AI}\frac{\partial^2 c_{AI}}{\partial z^2}, \tag{1a}$$

Region-II

$$-v_{zII}\frac{\partial c_{AII}}{\partial z} = \frac{\mathscr{D}_{AII}}{r}\frac{\partial}{\partial r}\left(r\frac{\partial c_{AII}}{\partial r}\right) + \mathscr{D}_{AII}\frac{\partial^2 c_{AII}}{\partial z^2}, \tag{1b}$$

In the above we have denoted by $Region-I$ to the space occupied in the inner compartment of the system, *i.e.*, $r \in (0, r_1)$ and $z \in (0, L)$; whereas $Region-II$ represents the annular compartment, *i.e.*, $r \in (r_1, r_2)$ and $z \in (0, L)$. In this way, $\mathscr{D}_{AI}$ and $\mathscr{D}_{AII}$ represent the molecular diffusivities of oxygen in helium and in air, respectively. The minus sign in Eq. (1b) follows from adopting counter-current operation conditions.

For momentum transport, the governing equations are,

Region-I

$$0 = \frac{\partial p_I}{\partial z} - \rho_I g + \frac{\mu_I}{r}\frac{\partial}{\partial r}\left(r\frac{\partial v_{zI}}{\partial r}\right), \tag{2a}$$

Region-II

$$0 = -\frac{\partial p_{II}}{\partial z} + \rho_{II} g + \frac{\mu_{II}}{r}\frac{\partial}{\partial r}\left(r\frac{\partial v_{zII}}{\partial r}\right), \tag{2b}$$

The differential equations (1), (2) are subject to the following boundary conditions

$$at\ \ z = 0, \quad c_{AI} = c_{AI0};\ \frac{\partial c_{AII}}{\partial z} = 0;\ p_I = p_{I0};\ p_{II} = p_{II0} \tag{3a}$$

$$at\ \ z = L, \quad \frac{\partial c_{AI}}{\partial z} = 0;\ c_{AII} = c_{AIIL};\ p_I = p_{IL};\ p_{II} = p_{IIL} \tag{3b}$$

$$at\ \ r = r_1, \quad \mathscr{D}_{AI}\frac{\partial c_{AI}}{\partial r} = \mathscr{D}_{AII}\frac{\partial c_{AII}}{\partial r} \tag{3c}$$

$$at\ \ r = r_1, \quad -\mathscr{D}_{AI}\frac{\partial c_{AI}}{\partial r} = P(c_{AI} - c_{AII}) \tag{3d}$$

$$at\ \ r = r_1, \quad v_{zI} = 0;\ v_{zII} = 0 \tag{3e}$$

$$at\ \ r = r_2, \quad \mathscr{D}_{AII}\frac{\partial c_{AII}}{\partial r} = 0 \tag{3f}$$

$$at\ \ r = r_2, \quad v_{zII} = 0 \tag{3g}$$

Naturally the concentration and velocity fields are constrained to be defined for all r and z. According to the Neumann-type boundary conditions in eqs. (3a) and (3b), the system length, L, is assumed large enough so that, at the outlets, the concentration of oxygen in the inner and annular regions are no longer a function of the z position. As assumed above, the porous membrane is regarded as a boundary where we have imposed continuity of the mass flux and a jump in the concentration (see eqs. 3c and 3d). In specific, the boundary condition in Eq. (3d) appears to be consistent with previous studies (see Section 2 in Wang *et al.*, 2004). In addition, possible slips of the velocity fields at the fluid-porous medium boundaries are neglected according to Eq. (3e). Finally, the shell wall is assumed impermeable to mass transfer (see Eq. 3f) and non-slip conditions are also assumed to apply (see Eq. 3g).

2.1 Velocity fields

Since flow is fully developed and momentum transport is assumed independent of mass transfer, one may solve the corresponding boundary-value problems to obtain the following well-known expressions (for details, see Sections 2.3 and 2.4 in Bird *et al.*, 2007),

$$v_{zI} = \frac{(\mathscr{P}_{I0} - \mathscr{P}_{IL})r_1^2}{4\mu_I L}\left[1 - \left(\frac{r}{r_1}\right)^2\right] \tag{4a}$$

$$v_{zII} = \frac{(\mathscr{P}_{II0} - \mathscr{P}_{IIL})r_2^2}{4\mu_{II} L}\left[1 - \left(\frac{r}{r_2}\right)^2 - \left(1 - \frac{r_1^2}{r_2^2}\right)\frac{\ln r/r_2}{\ln r_1/r_2}\right] \tag{4b}$$

here $\mathscr{P}_i = p_i - \rho_i g$ $(i = I, II)$. These expressions will be used in the following section that is devoted to the derivation of the upscaled model. From this point on, the velocity fields will be treated as known functions of r.

3 Upscaling

3.1 Unclosed model

As briefly described in the introduction, the upscaling process consists of several steps, which will be detailed in this section. Since we are interested in the cross-sectional averaged concentration, we define the averaging operator,

$$\langle c_A \rangle = \frac{1}{\pi r_2^2}\int_{\theta=0}^{\theta=2\pi}\int_{r=0}^{r=r_2} c_A r dr d\theta = \frac{2}{r_2^2}\int_{r=0}^{r=r_2} c_A r dr \tag{5}$$

Notice that the second equality holds under the axi-symmetric assumption for mass transport. Furthermore, since

$$c_A = \begin{cases} c_{AI}, & \forall r \in [0, r_1] \\ c_{AII}, & \forall r \in [r_1, r_2] \end{cases} \tag{6}$$

we may decompose Eq. (5) into

$$\langle c_A \rangle = \left(\frac{r_1}{r_2}\right)^2 \langle c_{AI} \rangle^I + \left[1 - \left(\frac{r_1}{r_2}\right)^2\right]\langle c_{AII} \rangle^{II} \tag{7}$$

Here we introduced the averaging operators,

$$\langle c_{AI} \rangle^I = \frac{2}{r_1^2}\int_{r=0}^{r=r_1} c_{AI} r dr \tag{8a}$$

$$\langle c_{AII} \rangle^{II} = \frac{2}{r_2^2 - r_1^2}\int_{r=r_1}^{r=r_2} c_{AII} r dr \tag{8b}$$

Notice that the averaged concentrations are only functions of the z-direction. In the following, we will refer to the average concentration defined in Eq. (5) as the *weighted averaged concentration* and to the concentrations defined in eqs. (8) as the *average concentrations in each region*. Our goal in the following paragraphs is to derive the governing differential equations for $\langle c_{AI} \rangle^I$ and $\langle c_{AII} \rangle^{II}$. In an equilibrium approach, one would derive the governing expression for $\langle c_A \rangle$ and find the conditions under which this average concentration is a good representation for the process. However, since we are pursuing a non-equilibrium approach, we are interested in deriving the governing expressions for $\langle c_{AI} \rangle^I$ and $\langle c_{AII} \rangle^{II}$.

For the time being, let us direct the attention to the inner region of the system, and apply the averaging operator defined in Eq. (8a) to Eq. (1a) to obtain,

$$\left\langle v_{zI}\frac{\partial c_{AI}}{\partial z}\right\rangle^I = \mathscr{D}_{AI}\left\langle \frac{1}{r}\frac{\partial}{\partial r}\left(r\frac{\partial c_{AI}}{\partial r}\right)\right\rangle^I + \mathscr{D}_{AI}\frac{d^2\langle c_{AI}\rangle^I}{dz^2} \tag{9}$$

here we have assumed that the molecular diffusivity is a constant within the averaging domain. In addition, since the limits of integration are independent of the z-direction, we freely exchanged differentiation and integration in the last term on the right-hand side of Eq. (9).

On the basis of the definition given in Eq. (8a) we can further develop the average of the first diffusive term in Eq. (9) as follows,

$$\begin{aligned}\mathscr{D}_{AI}\left\langle \frac{1}{r}\frac{\partial}{\partial r}\left(r\frac{\partial c_{AI}}{\partial r}\right)\right\rangle^I &= \frac{2\mathscr{D}_{AI}}{r_1^2}\int_{r=0}^{r=r_1}\frac{\partial}{\partial r}\left(r\frac{\partial c_{AI}}{\partial r}\right)dr \\ &= \frac{2\mathscr{D}_{AI}}{r_1}\left.\frac{\partial c_{AI}}{\partial r}\right|_{r=r_1}\end{aligned} \tag{10}$$

Directing our attention to the convective term in Eq. (9), we find it convenient to decompose the concentration and velocity fields in terms of the corresponding averages and spatial deviations according to the following expressions (Gray, 1975),

$$c_{AI} = \langle c_{AI} \rangle^I + \tilde{c}_{AI} \tag{11a}$$

$$v_{zI} = \langle v_{zI} \rangle^I + \tilde{v}_{zI} \tag{11b}$$

Since we are pursuing a local upscaled model (see Wood and Valdés-Parada, 2013 for a discussion about

local and nonlocal upscaled models), it is necessary to impose the following average constraints to the deviation fields:

$$\langle \tilde{v}_{zI} \rangle^I = 0; \quad \langle \tilde{c}_{AI} \rangle^I = 0 \tag{12}$$

Under these circumstances, we may express the convective term in Eq. (9) as follows

$$\left\langle v_{zI} \frac{\partial c_{AI}}{\partial z} \right\rangle^I = \langle v_{zI} \rangle^I \frac{d\langle c_{AI} \rangle^I}{dz} + \left\langle \tilde{v}_{zI} \frac{\partial \tilde{c}_{AI}}{\partial z} \right\rangle^I \tag{13}$$

here we have taken into account the fact that average quantities are only functions of the z-direction as well as the average constraints in Eq. (12).

Substitution of eqs. (10) and (13) into Eq. (9) yields

$$\langle v_{zI} \rangle^I \frac{d\langle c_{AI} \rangle^I}{dz} + \underbrace{\left\langle \tilde{v}_{zI} \frac{\partial \tilde{c}_{AI}}{\partial z} \right\rangle^I}_{convective\ \ filter} = \mathscr{D}_{AI} \frac{d^2 \langle c_{AI} \rangle^I}{dz^2} + \underbrace{\frac{2\mathscr{D}_{AI}}{r_1} \left. \frac{\partial \tilde{c}_{AI}}{\partial r} \right|_{r=r_1}}_{diffusive\ \ filter} \tag{14a}$$

Notice that we have used the concentration spatial decomposition on the last term of the above result taking into account the fact that $\partial \langle c_{AI} \rangle^I / \partial r = 0$. In addition, we have regarded the terms involving deviations fields as filters of information from the microscale (Whitaker, 1999).

Repeating the steps followed so far to the annular region, we obtain

$$-\langle v_{zII} \rangle^{II} \frac{d\langle c_{AII} \rangle^{II}}{dz} - \left\langle \tilde{v}_{zII} \frac{\partial \tilde{c}_{AII}}{\partial z} \right\rangle^{II} = \mathscr{D}_{AII} \frac{d^2 \langle c_{AII} \rangle^{II}}{dz^2} - \frac{2\mathscr{D}_{AII} r_1}{r_2^2 - r_1^2} \left. \frac{\partial \tilde{c}_{AII}}{\partial r} \right|_{r=r_1} \tag{14b}$$

Indeed, this expression takes into account the boundary condition given in Eq. (3f). At this point in the analysis, one can not make further progress until the velocity and concentration deviations fields are available. The process of deriving expressions for the deviations in terms of averaged quantities is known as *closure* (Whitaker, 1999) and it will be performed in the following paragraphs.

3.2 Closure problem

For momentum transport, since we have the pointwise velocity fields, we may apply the averaging operators given in eqs. (8a) and (8b) to eqs. (4a) and (4b), respectively, to obtain,

$$\langle v_{zI} \rangle^I = \frac{(\mathscr{P}_{I0} - \mathscr{P}_{IL}) r_1^2}{8\mu_I L} \tag{15a}$$

$$\langle v_{zII} \rangle^{II} = \frac{(\mathscr{P}_{II0} - \mathscr{P}_{IIL}) r_2^2}{8\mu_{II} L} \left(1 + \xi_1^2 + \frac{1 - \xi_1^2}{\ln \xi_1} \right) \tag{15b}$$

As a matter of convenience, we introduce the dimensionless parameter

$$\xi_1 = \frac{r_1}{r_2} \tag{16}$$

In terms of the averaged velocities, we may rewrite eqs. (4a) and (4b) as follows,

$$v_{zI} = 2\langle v_{zI} \rangle^I \left[1 - \left(\frac{\xi}{\xi_1} \right)^2 \right] \tag{17a}$$

$$v_{zII} = \langle v_{zII} \rangle^{II} \left[\frac{(\xi_1^2 - 1) \ln \xi / \xi_1 + \left(\xi_1^2 - \xi^2 \right) \ln \xi_1}{(1 + \xi_1^2) \ln \xi_1 + 1 - \xi_1^2} \right] \tag{17b}$$

In the above expressions we introduce the dimensionless variable

$$\xi = \frac{r}{r_2} \tag{18}$$

In this way, subtracting $\langle v_{zI} \rangle^I$ on both sides of Eq. (17a) yields,

$$\tilde{v}_{zI} = \langle v_{zI} \rangle^I \left[1 - 2 \left(\frac{\xi}{\xi_1} \right)^2 \right] \tag{19a}$$

Accordingly, the result of subtracting $\langle v_{zII} \rangle^{II}$ on both sides of Eq. (17b) is,

$$\frac{\tilde{v}_{zII}}{\langle v_{zII} \rangle^{II}} = 2 \left[\frac{(\xi_1^2 - 1)(2 \ln \xi / \xi_1 + 1) + \left(\xi_1^2 - 2\xi^2 - 1 \right) \ln \xi_1}{(1 + \xi_1^2) \ln \xi_1 + 1 - \xi_1^2} \right] = \frac{1}{\delta} \left(-2 \ln \xi - 2\chi \xi^2 + \ln \xi_1 - 1 \right) \tag{19b}$$

For the sake of simplicity we introduce,

$$\chi = \frac{\ln \xi_1}{1 - \xi_1^2}; \quad \delta = (1 + \xi_1^2)\chi + 1 \tag{20}$$

The results in eqs. (19a) and (19b) are the desired results for the velocity deviations. In addition, it can be proved that the expressions in eqs. (19a) and (19b) satisfy the average constraints $\langle \tilde{v}_{zI} \rangle^I = \langle \tilde{v}_{zII} \rangle^{II} = 0$.

It should be stressed that the derivation of the velocity deviations was straightforward because the

pointwise velocity fields were available. However, the same is not true for mass transfer. In this case, it is more convenient to derive and solve the governing boundary-value problem for the concentration deviations. The derivation of this problem is provided in Appendix A and it is given by the differential equations (A.6) and (A.7), which are subject to the boundary conditions given in (A.9) and the average constraints in Eq. (A.10). The length-scale constraints supporting the derivation of this problem are

$$Pe^I \frac{r_1}{L} \ll 1; \quad Pe^{II} \frac{r_2}{L} \ll 1; \quad r_1^2 \ll L^2; \quad r_2^2 \ll L^2 \tag{21}$$

which are expressed in terms of two Péclet numbers $Pe^I \equiv \langle v_{zI}\rangle^I r_1/\mathscr{D}_{AI}$ and $Pe^{II} \equiv \langle v_{zII}\rangle^{II} r_2/\mathscr{D}_{AII}$. The constraints provided above bound the range of applicability of the upscaled model and they play a crucial role in the comparison with direct numerical simulations as will be shown in Section 4.

As stressed in Appendix A, the closure problem is linear and it is conveniently written in terms of volume and surface sources; hence, the following superposition solutions can be proposed

$$\tilde{c}_{AI} = b_{I,I}(r)\frac{d\langle c_{AI}\rangle^I}{dz} + b_{I,II}(r)\frac{d\langle c_{AII}\rangle^{II}}{dz} + s_I(r)\left(\langle c_{AI}\rangle^I - \langle c_{AII}\rangle^{II}\right) \tag{22a}$$

$$\tilde{c}_{AII} = b_{II,I}(r)\frac{d\langle c_{AI}\rangle^I}{dz} + b_{II,II}(r)\frac{d\langle c_{AII}\rangle^{II}}{dz} + s_{II}(r)\left(\langle c_{AI}\rangle^I - \langle c_{AII}\rangle^{II}\right) \tag{22b}$$

Here the functions b and s are closure variables that can be predicted from the solution of the closure problem derived in Appendix A. The details of the analytical solution of the closure problem are provided in Appendix B. Comparing eqs. (B.6) with eqs. (22), it results that

$$\frac{b_{I,I}}{r_2} = \frac{Pe^I\xi_1}{4}\left(\frac{(2\alpha+1)\xi^2}{\xi_1^2} - \frac{\xi^4}{2\xi_1^4} - \frac{1}{3} - \alpha\right) \tag{23a}$$

$$\frac{b_{I,II}}{r_2} = -\frac{Pe^{II}\beta}{24\alpha}s_I \tag{23b}$$

$$s_I = 12\alpha\left(\frac{\xi^2}{\xi_1^2} - \frac{1}{2}\right) \tag{23c}$$

$$\frac{b_{II,I}}{r_2} = \frac{Pe^I\xi_1}{24}s_{II} \tag{23d}$$

$$\frac{b_{II,II}}{r_2} = \frac{Pe^{II}}{\delta}\left[\frac{\xi^2}{2}\ln\frac{\xi}{\xi_1} + \frac{\xi^4\chi}{8} - \frac{\frac{\gamma_1\xi^2}{4} + \gamma_2\ln\xi + \gamma_0}{1-\xi_1^2}\right] \tag{23e}$$

$$s_{II} = \frac{24\mathscr{D}_{AI}\alpha}{\left(1-\xi_1^2\right)\mathscr{D}_{AII}}\left(\ln\xi - \frac{\xi^2}{2} + \xi_1^2\chi + \frac{3+\xi_1^2}{4}\right) \tag{23f}$$

The parameters involved in these equations are available in Appendix B (see eqs. B.5 and B.7). Among these parameters, it is worth highlighting that the coefficients α and β, as defined in eqs. (B.5b) and (B.5c), are directly proportional to the modified Sherwood number,

$$Sh = \frac{\mathrm{P}\, r_2}{\mathscr{D}_{AI}} \tag{24}$$

Consequently, an increment of the membrane permeability, P will have a proportional effect in the values of α and β. This observation will be relevant in subsequent paragraphs. Before moving on, it is worth noting that the modified Sherwood number, as defined in Eq. (24) can be further developed as follows,

$$Sh = \frac{\mathrm{P}\,\ell}{D_{eff}}\frac{D_{eff}}{\mathscr{D}_{AI}}\frac{r_2}{\ell} \tag{25}$$

where the product $\mathrm{P}\,\ell/D_{eff}$ can be identified as the membrane Sherwood number, with D_{eff} being the effective diffusivity of oxygen in the porous membrane. Certainly, the membrane Sherwood number and the ratio $\frac{D_{eff}}{\mathscr{D}_{AI}}$ are dimensionless quantities that are not larger than 1; however the ratio r_2/ℓ is larger than 1. From the above, it seems reasonable to allow the modified Sherwood number to acquire values that are either larger than or smaller than the unity.

3.3 *Closed model*

Now that we have expressions for the concentration and velocity deviations, we can return to the unclosed expressions given in eqs. (14a) and (14b) and substitute the deviations fields in the corresponding integral terms in order to obtain,

Region-I:

$$\left(\langle v_{zI}\rangle^I + \langle \tilde{v}_{zI} s_I\rangle^I - \frac{2\mathscr{D}_{AI}}{r_1}\left.\frac{\partial b_{I,I}}{\partial r}\right|_{r_1}\right)\frac{d\langle c_{AI}\rangle^I}{dz} - \left(\langle \tilde{v}_{zI} s_I\rangle^I + \frac{2\mathscr{D}_{AI}}{r_1}\left.\frac{\partial b_{I,II}}{\partial r}\right|_{r_1}\right)\frac{d\langle c_{AII}\rangle^{II}}{dz}$$
$$= \left(\mathscr{D}_{AI} - \langle \tilde{v}_{zI} b_{I,I}\rangle^I\right)\frac{d^2\langle c_{AI}\rangle^I}{dz^2} - \langle \tilde{v}_{zI} b_{I,II}\rangle^I\frac{d^2\langle c_{AII}\rangle^{II}}{dz^2} + \frac{2\mathscr{D}_{AI}}{r_1}\left.\frac{\partial s_I}{\partial r}\right|_{r_1}\left(\langle c_{AI}\rangle^I - \langle c_{AII}\rangle^{II}\right) \tag{26a}$$

Region-II:

$$\left[-\langle v_{zII}\rangle^{II} + \langle \tilde{v}_{zII} s_{II}\rangle^{II} + \frac{2\mathscr{D}_{AII} r_1}{\left(r_2^2 - r_1^2\right)}\left.\frac{\partial b_{II,II}}{\partial r}\right|_{r_1}\right]\frac{d\langle c_{AII}\rangle^{II}}{dz} + \left[-\langle \tilde{v}_{zII} s_{II}\rangle^{II} + \frac{\mathscr{D}_{AII} r_1}{\left(r_2^2 - r_1^2\right)}\left.\frac{\partial b_{II,I}}{\partial r}\right|_{r_1}\right]\frac{d\langle c_{AI}\rangle^I}{dz}$$
$$= \left(\mathscr{D}_{AII} + \langle \tilde{v}_{zII} b_{II,II}\rangle^{II}\right)\frac{d^2\langle c_{AII}\rangle^{II}}{dz^2} + \langle \tilde{v}_{zII} b_{II,I}\rangle^{II}\frac{d^2\langle c_{AI}\rangle^I}{dz^2} - \frac{2\mathscr{D}_{AII} r_1}{\left(r_2^2 - r_1^2\right)}\left.\frac{\partial s_{II}}{\partial r}\right|_{r_1}\left(\langle c_{AI}\rangle^I - \langle c_{AII}\rangle^{II}\right) \tag{26b}$$

The above equations can be further developed after performing the corresponding integration and differentiation operations, the resulting expressions are written as follows

Region-I:

$$v_{I,I}\frac{d\langle c_{AI}\rangle^I}{dz} - v_{I,II}\frac{d\langle c_{AII}\rangle^{II}}{dz} = D_{I,I}\frac{d^2\langle c_{AI}\rangle^I}{dz^2} - D_{I,II}\frac{d^2\langle c_{AII}\rangle^{II}}{dz^2} - \frac{h^{I,II}}{A_I}\left(\langle c_{AI}\rangle^I - \langle c_{AII}\rangle^{II}\right) \tag{27a}$$

Region-II:

$$-v_{II,II}\frac{d\langle c_{AII}\rangle^{II}}{dz} - v_{II,I}\frac{d\langle c_{AI}\rangle^I}{dz} = D_{II,II}\frac{d^2\langle c_{AII}\rangle^{II}}{dz^2} - D_{II,I}\frac{d^2\langle c_{AI}\rangle^I}{dz^2} + \frac{h^{I,II}}{A_{II}}\left(\langle c_{AI}\rangle^I - \langle c_{AII}\rangle^{II}\right) \tag{27b}$$

Here we have identified the following effective-medium velocity and dispersion coefficients,

$$v_{I,I} = \langle v_{zI}\rangle^I(1-4\alpha); \quad v_{I,II} = -2\langle v_{z,I}\rangle^I\left(\alpha + \frac{Pe^{II}\beta}{Pe^I\xi_1}\right);$$
$$\frac{v_{II,I}}{\langle v_{zII}\rangle^{II}} = \frac{\langle \tilde{v}_{zII} s_{II}\rangle^{II}}{\langle v_{zII}\rangle^{II}} - \frac{\langle v_{zI}\rangle^I}{\langle v_{zII}\rangle^{II}}\frac{2\xi_1^2\alpha}{\left(1-\xi_1^2\right)} \tag{28a}$$

$$\frac{v_{II,II}}{\langle v_{zII}\rangle^{II}} = 1 - \frac{\langle \tilde{v}_{zII} s_{II}\rangle^{II}}{\langle v_{zII}\rangle^{II}} + \frac{\xi_1^2\left[\xi_1^2 - 1 + \gamma_1 - \xi_1^2\ln\xi_1 + \frac{2\gamma_2}{\xi_1^2}\right]}{\left(1-\xi_1^2\right)^2\delta} \tag{28b}$$

$$\frac{D_{I,I}}{\mathscr{D}_{AI}} = 1 + \frac{\left(Pe^I\right)^2(1+4\alpha)}{48}; \quad D_{I,II} = \frac{Pe^{II}Pe^I\mathscr{D}_{AI}\beta}{12\xi_1};$$
$$\frac{D_{II,II}}{\mathscr{D}_{AII}} = 1 + \frac{\langle \tilde{v}_{zII} b_{II,II}\rangle^{II}}{\mathscr{D}_{AII}}; \quad D_{II,I} = -\langle \tilde{v}_{zII} b_{II,I}\rangle^{II} \tag{28c}$$

Moreover, we introduced the interfacial mass transport coefficient as

$$h^{I,II} = -48\pi\alpha\mathscr{D}_{AI} = \left[\frac{6}{\mathscr{D}_{AI}} + \frac{24}{Pr_1} + \frac{1}{\mathscr{D}_{AII}}\left(\frac{24\chi + 6\left(3-\xi_1^2\right)}{\xi_1^2 - 1}\right)\right]^{-1}\left(\frac{1}{48\pi}\right)^{-1} \tag{28d}$$

as well as the area coefficients

$$A_I = r_2^2\pi\xi_1^2; \quad A_{II} = r_2^2\pi\left(1-\xi_1^2\right) \tag{28e}$$

The sign choices for the coefficients defined in eqs. (27) were decided on the basis of defining all effective medium coefficients as positive-definite quantities. In addition, the analytical expressions of the integral terms

$$\frac{\langle \tilde{v}_{zII} b_{II,II} \rangle^{II}}{\mathscr{D}_{AII}} = \left(\frac{Pe^{II}}{(1-\xi_1^2)\delta} \right)^2 \left\{ \begin{array}{l} \dfrac{\left(\xi_1^2-1\right)}{16}\left[1-\xi_1^4+2\ln\xi_1\left(1+\xi_1^4\right)\right] - \dfrac{\gamma_1}{4}\left[\xi_1^4\ln\xi_1+\dfrac{1-\xi_1^4}{4}\right] \\ -\dfrac{\ln\xi_1}{12}\left[-\xi_1^6\ln\xi_1-\dfrac{1-\xi_1^6}{6}\right]+\gamma_2\left[1-\xi_1^2+2\xi_1^2\ln\xi_1-2\xi_1^2(\ln\xi_1)^2\right] \\ +\ln\xi_1\left[\begin{array}{l}\dfrac{1}{3}\left[\ln\xi_1+\dfrac{1-\xi_1^6}{6}\right]-\gamma_1\dfrac{1-\xi_1^6}{6\left(\xi_1^2-1\right)} \\ +\dfrac{\left(1-\xi_1^8\right)\ln\xi_1}{16\left(\xi_1^2-1\right)}+\dfrac{\gamma_2}{\left(\xi_1^2-1\right)}\left(\xi_1^4\ln\xi_1+\dfrac{1-\xi_1^4}{4}\right)\end{array}\right] \\ +(1-\ln\xi_1)\left[\begin{array}{l}\dfrac{\left(1-\xi_1^2\right)}{4}\left(\ln\xi_1+\dfrac{1-\xi_1^4}{4}\right)+\gamma_1\dfrac{1-\xi_1^4}{8} \\ -\dfrac{\left(1-\xi_1^6\right)\ln\xi_1}{24}-\gamma_2\left(\xi_1^2\ln\xi_1+\dfrac{1-\xi_1^2}{2}\right)\end{array}\right] \end{array} \right\} \tag{29a}$$

$$\frac{\langle \tilde{v}_{zII} s_{II} \rangle^{II}}{\langle v_{z,II} \rangle^{II}} = \frac{-3\mathscr{D}_{AI}\alpha}{\delta\left(1-\xi_1^2\right)^2\mathscr{D}_{AII}} \left[\begin{array}{l} 9-\xi_1^2\left(8+\xi_1^2+\ln\xi_1\left(16\ln\xi_1-16-4\xi_1^2\right)\right) \\ -2\ln\xi_1\left(\dfrac{4\left(\xi_1^6-1\right)-12\xi_1^4\ln\xi_1}{3\left(\xi_1^2-1\right)}+\xi_1^2+1\right) \\ +2\left(1-\ln\xi_1\right)\left(\xi_1^2-1\right)\left(\xi_1^2+3-\dfrac{4\xi_1^2\ln\xi_1}{\left(\xi_1^2-1\right)}\right) \end{array} \right] \tag{29b}$$

$$\frac{\langle \tilde{v}_{zII} b_{II,I} \rangle^{II}}{\mathscr{D}_{AII}} = \frac{Pe^I Pe^{II}\xi_1}{24}\frac{\langle \tilde{v}_{zII} s_{II} \rangle^{II}}{\langle v_{z,II} \rangle^{II}} \tag{29c}$$

In the following section we will evaluate the capabilities of the macroscale model, as defined by eqs. (27), by comparing the predictions of the concentration profiles with those resulting by solving the microscale equations (*i.e.*, by performing *Direct Numerical Simulations* or DNS). Before performing this comparison, it is worth remarking some relevant features of the macroscale model and the associated coefficients:

- Mass transfer in each region is influenced by: convective and dispersive transport taking place in both regions as well as by the inter-regional mass exchange. The associated physical meaning of each effective medium coefficient is the following: $h^{I,II}$ is the interfacial mass transport coefficient that encompasses the influence of the porous membrane and can be analytically predicted from Eq. (28d). In fact, from this expression, it is clearly shown that this coefficient involves the inverse of the sum of diffusive and interfacial resistances in the membrane. $v_{I,I}$ and $v_{II,II}$ are the velocity fields in each region that are modified by the mass exchange caused by the porous membrane. As a matter of fact, in the limit as $\alpha \to 0$, it results that $v_{I,I} = \langle v_{zI} \rangle^I$ and $v_{II,II} = \langle v_{zII} \rangle^{II}$, respectively. The coefficients $v_{I,II}$ and $v_{II,I}$ can be thought of as the effective convective velocities exerted by the stream in Region II over the one in Region I and vice versa, respectively. These velocity coefficients are non-trivial functions of diffusion and convection in both regions and do not appear in the pointwise model because they are a direct result of the upscaling process. In a similar way, $D_{I,II}$ and $D_{II,I}$ are the dispersion coefficients that account

for the influence of this transport mechanism in Region II over Region I and vice versa, respectively and are the outcome of upscaling.

For cases in which the porous membrane exhibits little or null permeability to mass transfer, it follows immediately that h tends to zero. Therefore, from Eq. (28c), we note that $4\alpha \ll 1$, hence the dispersion in the inner region of the system, $D_{I,I}$ reduces to the classical expression deduced by Taylor (1953, 1954):

$$\frac{D_{I,I}}{\mathscr{D}_{AI}} = 1 + \frac{\left(Pe^I\right)^2}{48} \tag{30}$$

Under these conditions, we also have that $\beta \ll 1$, and thus the following identities hold

$$D_{I,II} = D_{II,I} = 0 \tag{31a}$$

$$v_{I,I} = \langle v_{zI}\rangle^I; \quad v_{I,II} = v_{II,I} = 0; \quad v_{II,II} = -\langle v_{zI}\rangle^{II} \tag{31b}$$

Therefore, the macroscale model reduces to the following set of uncoupled equations,

Region-I:

$$\langle v_{zI}\rangle^I \frac{d\langle c_{AI}\rangle^I}{dz} = D_{I,I}\frac{d^2\langle c_{AI}\rangle^I}{dz^2} \tag{32a}$$

Region-II:

$$-\langle v_{zI}\rangle^{II} \frac{d\langle c_{AII}\rangle^{II}}{dz} = D_{II,II}\frac{d^2\langle c_{AII}\rangle^{II}}{dz^2} \tag{32b}$$

which are the classical convection-dispersion expressions for flow in a tube and in the annular section of two tubes, respectively.

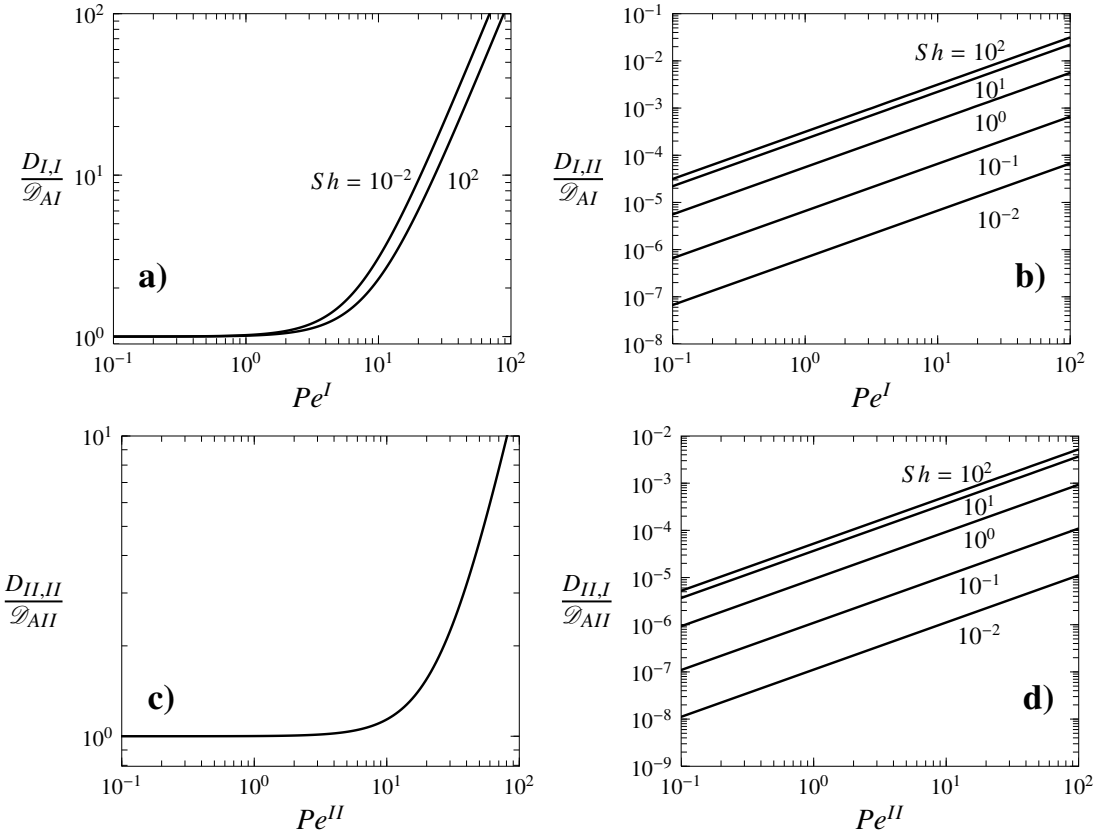

Fig. 2. Dependence of the dispersion coefficients with the Péclet and modified Sherwood numbers taking $\xi_1 = 0.5$, $L = 5r_2$, $\mathscr{D}_{AI}/\mathscr{D}_{AII} = 1$ and for a), b) $Pe^{II} = 1$ and for c), d) $Pe^I = 1$.

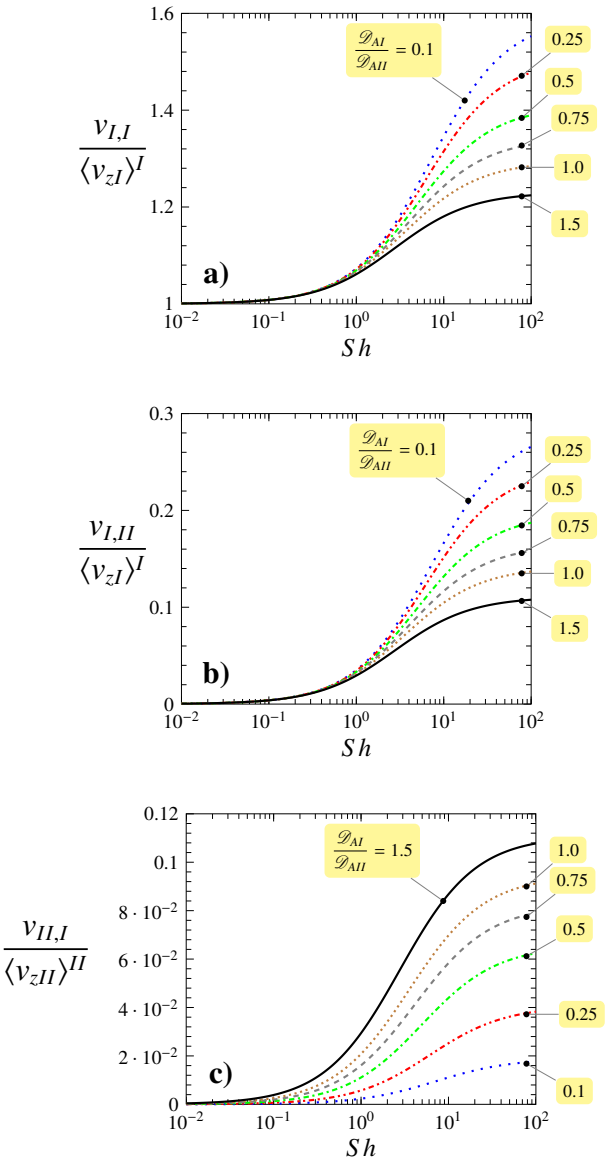

Fig. 3. Dependence of the effective velocity coefficients with the modified Sherwood number for several values of $\mathscr{D}_{AI}/\mathscr{D}_{AII}$, taking $\xi_1 = 0.5$, $L = 5r_2$ and $Pe^I = Pe^{II} = 1$.

- As shown in Fig. 2, the dispersion coefficients $D_{I,I}$, $D_{I,II}$, $D_{II,I}$ and $D_{II,II}$ are all functions of the Péclet numbers of both regions. We note that the functionality of $D_{I,I}$ with Pe^I and the one of $D_{II,II}$ with Pe^{II}, resembles the typical shape reported by Taylor (1953,1954). This tendency can be divided in two portions: the first one (for Péclet number values much smaller than 1) is

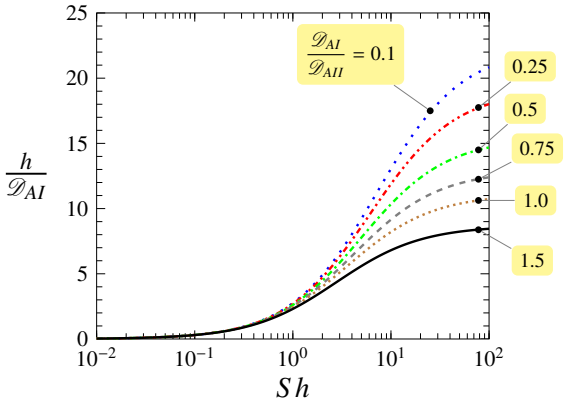

Fig. 4. Dependence of the interfacial transport coefficient with the modified Sherwood number for several values of $\mathscr{D}_{AI}/\mathscr{D}_{AII}$, taking $\xi_1 = 0.5$, $L = 5r_2$ and $Pe^I = Pe^{II} = 1$.

dominated by convection and thus the dispersion coefficient is equal to the molecular diffusivity. The second portion (for Péclet number values larger than 1) is dominated by diffusion and the dispersion coefficient rapidly increases with the Péclet number. Regarding the dependence of the dispersion coefficients with the membrane permeability we have, on the one hand, that the coefficients $D_{I,II}$ and $D_{II,I}$ are directly proportional to the Sherwood number and are highly sensitive to variations of this parameter. On the other hand, the dispersion coefficients $D_{I,I}$ and $D_{II,II}$ are practically insensitive to variations of Sh. This implies that cross-regional dispersion is, as expected, favored by the membrane permeability. The reason for the insensitivity of $D_{I,I}$ and $D_{II,II}$ with Sh is due to the fact that, for the conditions used in Fig. 2, α is, at most, on the order of 10^{-2}. Finally, it is worth noting that the values of $D_{I,I}$ and $D_{II,II}$ are orders of magnitude larger than those for $D_{I,II}$ and $D_{II,I}$.

- About the functionality of the effective velocity coefficients with the membrane permeability, we have, from the results provided in Fig. 3, that the coefficients $v_{I,I}$, $v_{I,II}$ and $v_{II,I}$ are increasing functions of the modified Sherwood number. In this figure we have not included a plot of $v_{II,II}$ versus Sh because this coefficient is independent of the membrane permeability. Although not shown in Fig. 3, it should be clear that $v_{I,I}$ and $v_{I,II}$ are directly proportional to Pe^I, whereas $v_{II,I}$ and $v_{II,II}$ are directly proportional

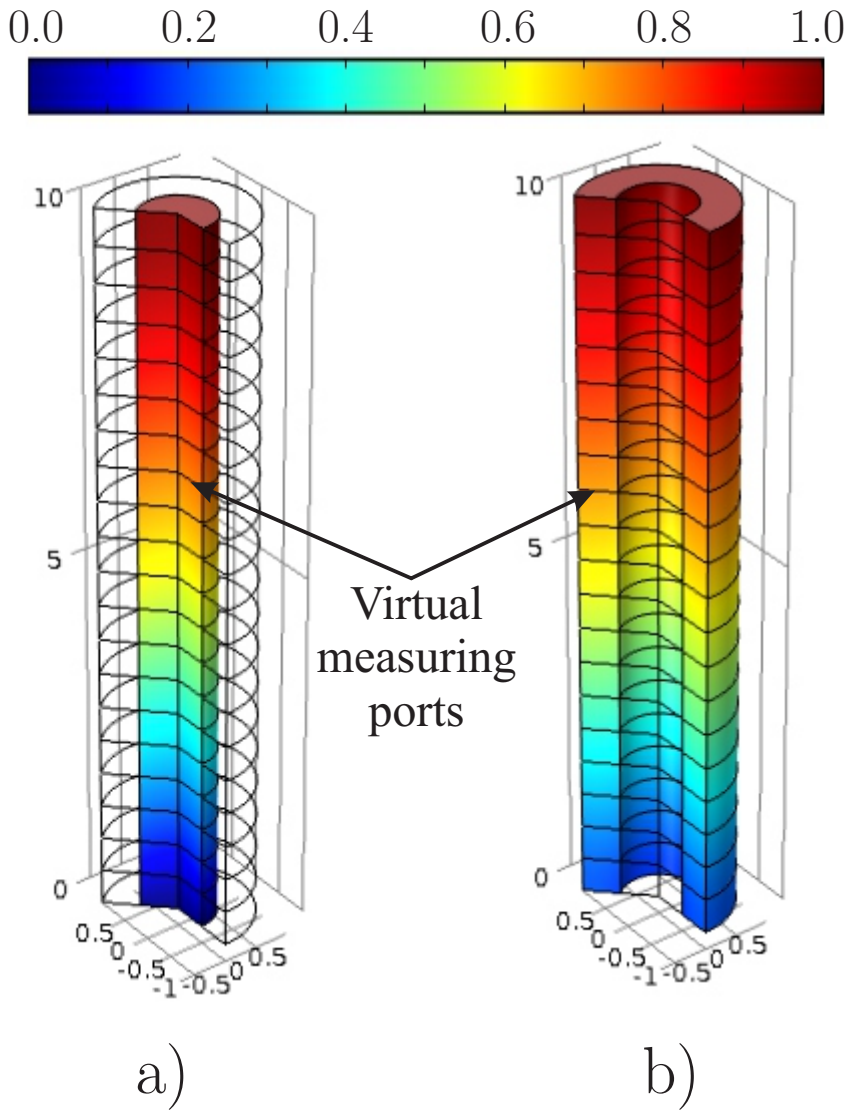

Fig. 5. Example of the dimensionless microscale concentration fields in a) the tube (Region-I) and b) the shell (Region-II) taking $\xi_1 = 0.5$, $r_2/L = 0.1$, $\mathscr{D}_{AI}/\mathscr{D}_{AII} = 1$ and $Pe^I = Pe^{II} = 1$. The virtual measuring ports are cross-sectional cuts along the vertical axis in the tubular and annular regions.

to Pe^{II}. In Fig. 3, we have also shown the dependence of the velocity coefficients with the ratio of diffusivities $\mathscr{D}_{AI}/\mathscr{D}_{AII}$, we observe that, for $Sh > 1$, $v_{I,I}$ and $v_{I,II}$ are inversely proportional to this ratio. In other words, the convective velocities in Region I are favored when the oxygen diffuses more freely in Region II than in Region I and the opposite is true for $v_{II,I}$. Finally, the interfacial mass transport coefficient is an increasing function of the modified Sherwood number as shown in Fig. 4. Interestingly, the functionality with the ratio of diffusivities $\mathscr{D}_{AI}/\mathscr{D}_{AII}$ is the same displayed by $v_{I,I}$ and $v_{I,II}$ as shown in Figs. 3a and 3b.

4 Comparison with Direct Numerical Simulations

In this section, we test the predictive capabilities of the upscaled model by comparing the average concentration profiles with those resulting from solving the pointwise model as defined by eqs. (1) and (3). In all the computations reported in this section we

took $c_{AI0} = 0$, implying that the noble gas current is always fed free from oxygen; in addition, we assume that the oxygen fed in the shell section has a constant concentration, c_{AIIL}. With this in mind, from this point on, we present the results in terms of the dimensionless concentrations,

$$U_{AI} = \frac{c_{AI}}{c_{AIIL}}; \quad U_{AII} = \frac{c_{AII}}{c_{AIIL}} \tag{33}$$

The pointwise model was numerically solved using the finite element method with the commercial software *Comsol Multiphysics* 4.3b. In the solution process we employed adaptive mesh refinements algorithms, provided in the software in order to make the solution independent of the number of mesh elements. In Fig. 5 we provide an example of the solution of this model for a permeator having an aspect ratio of $L = 10r_2$. Notice that, especially at the bottom of the system, the concentration profiles in each region of the system are clearly different, thus supporting our assumption of local mass non-equilibrium. As shown in the figure, we incorporated several *virtual measuring ports* along the equipment in order to compute the cross-sectional dimensionless averaged concentrations $\langle U_{AI}\rangle^I$ and $\langle U_{AII}\rangle^{II}$. Although in an actual experimental setup, it may not be possible to have plenty measuring ports (usually measurements are performed only at the inlets and outlets of the system), in this work we find it convenient to incorporate these *sensors* in order to have information about the concentration profiles inside the system.

Due to the non-trivial coupling of the upscaled concentrations in eqs. (27), we solved the upscaled model numerically subject to the following boundary conditions,

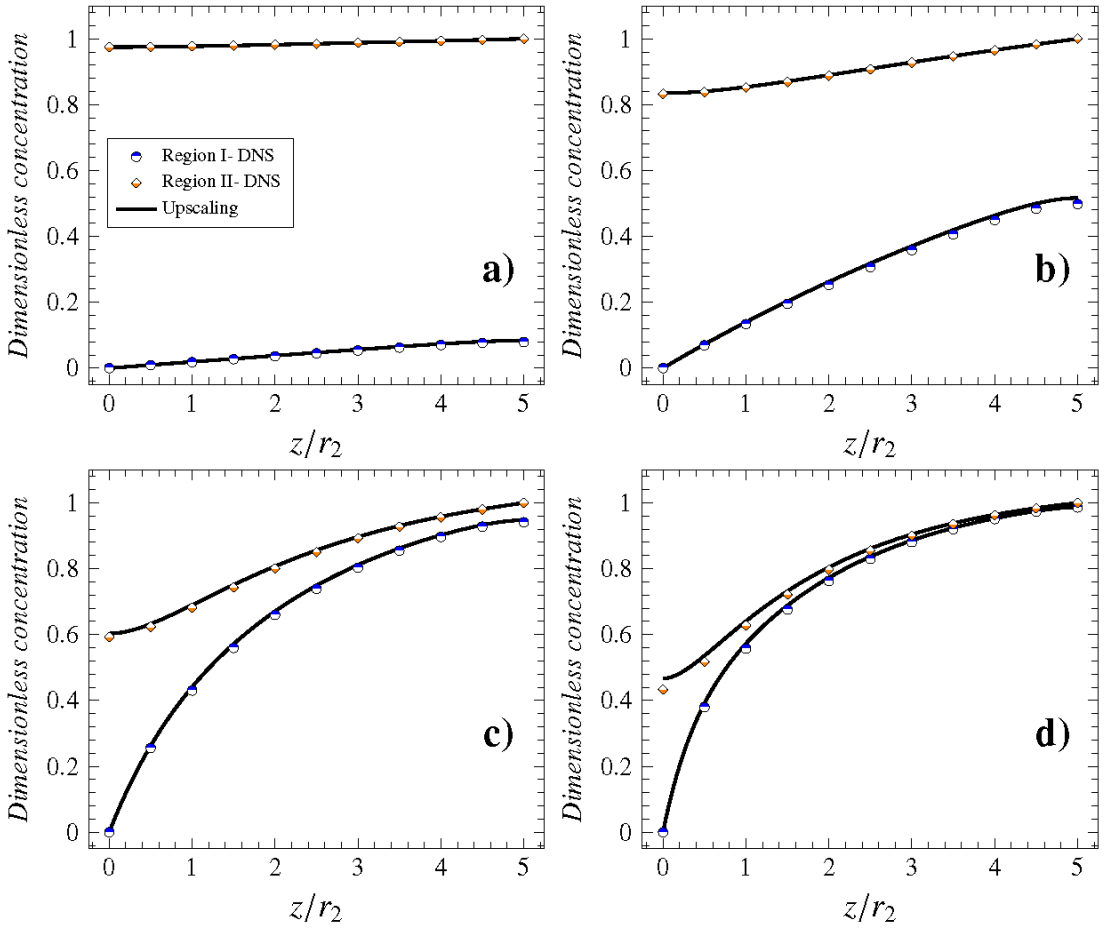

Fig. 6. Dimensionless average concentration profiles obtained with direct numerical simulations (DNS) and upscaling for a) Sh = 0.01, b) Sh = 0.1, c) Sh = 1 and d) Sh = 10, taking $\xi_1 = 0.5$, $L = 5r_2$, $\mathscr{D}_{AI}/\mathscr{D}_{AII} = 0.5$ and $Pe^I = Pe^{II} = 1$.

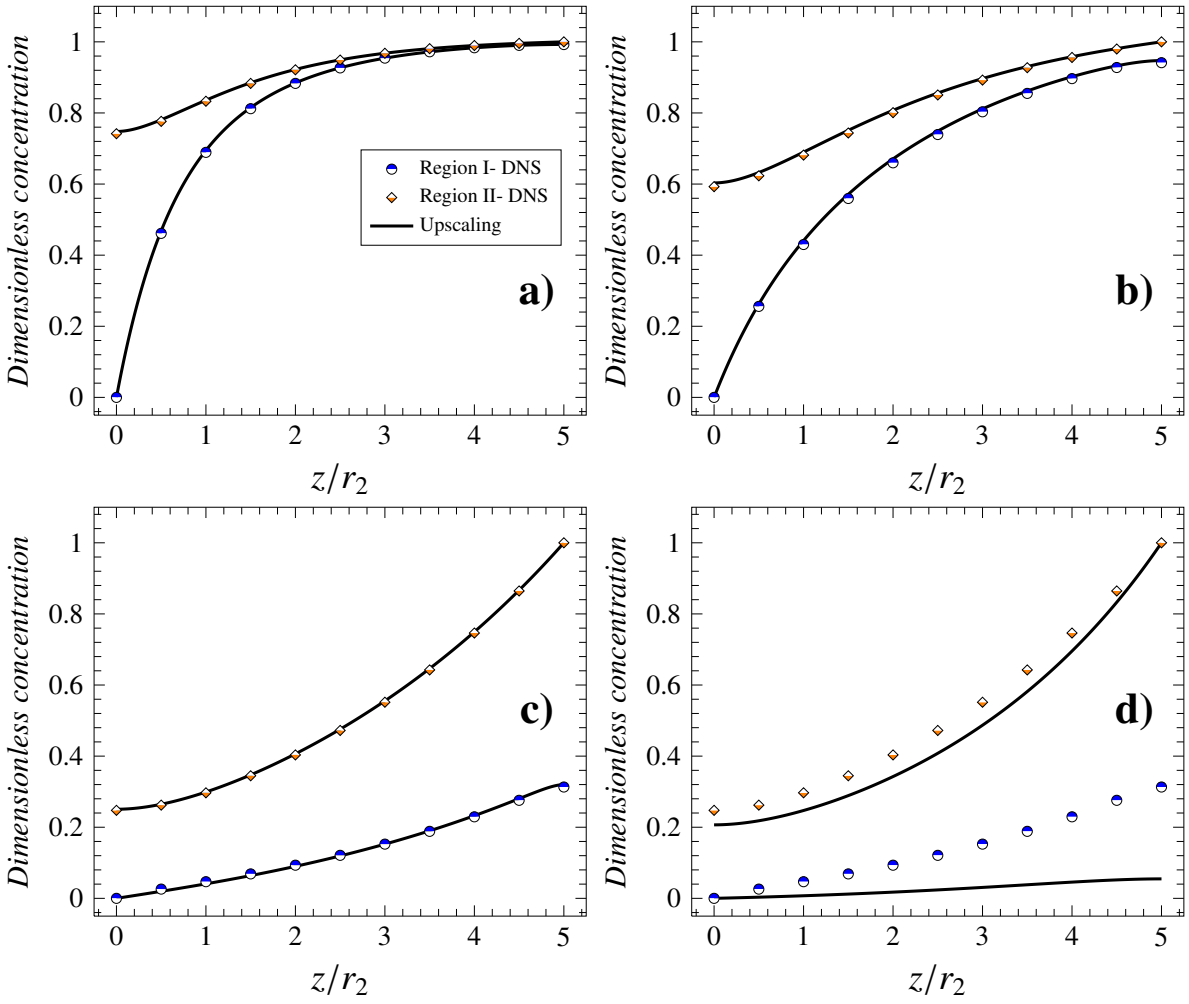

Fig. 7. Dimensionless average concentration profiles obtained with direct numerical simulations (DNS) and upscaling for a) $Pe^I = 0.1$, b) $Pe^I = 1$, c) $Pe^I = 10$ and d) $Pe^I = 100$, taking $\xi_1 = 0.5$, $L = 5r_2$, $\mathscr{D}_{AI}/\mathscr{D}_{AII} = 0.5$, $Sh = 1$ and $Pe^{II} = 1$.

$$at\ \ z = 0, \quad \langle U_{AI}\rangle^I = 0;\ \frac{d\langle U_{AII}\rangle^{II}}{dz} = 0; \tag{34a}$$

$$at\ \ z = L, \quad \frac{d\langle U_{AI}\rangle^I}{dz} = 0;\ \langle U_{AII}\rangle^{II} = 1; \tag{34b}$$

using finite differences schemes involving, as in the case of the microscale problem, adaptive mesh refinements schemes. In figs. 6-9, we provide several plots comparing the cross-sectional averaged concentration profiles arising from the upscaled model and those being computed from the virtual measuring ports in the DNS by varying the modified Sherwood number (Fig. 6), the Péclet numbers associated to Regions-I and -II (Figs. 7 and 8, respectively) and the ratio of molecular diffusivities $\mathscr{D}_{AI}/\mathscr{D}_{AII}$ (Fig. 9). For the sake of simplicity, in all the computations we took $\xi_1 = 0.5$ and $L = 5r_2$. Concerning these results, the following comments are in order:

- From the results in Fig. 6, we appreciate that, as the membrane permeability increases (*i.e.*, as the modified Sherwood number grows), there is a better exchange of oxygen between both regions and it is thus reasonable to think that, for $Sh > 1$, the concentration of oxygen in Region-I approaches the unity at the exit (as shown in Fig. 6d).

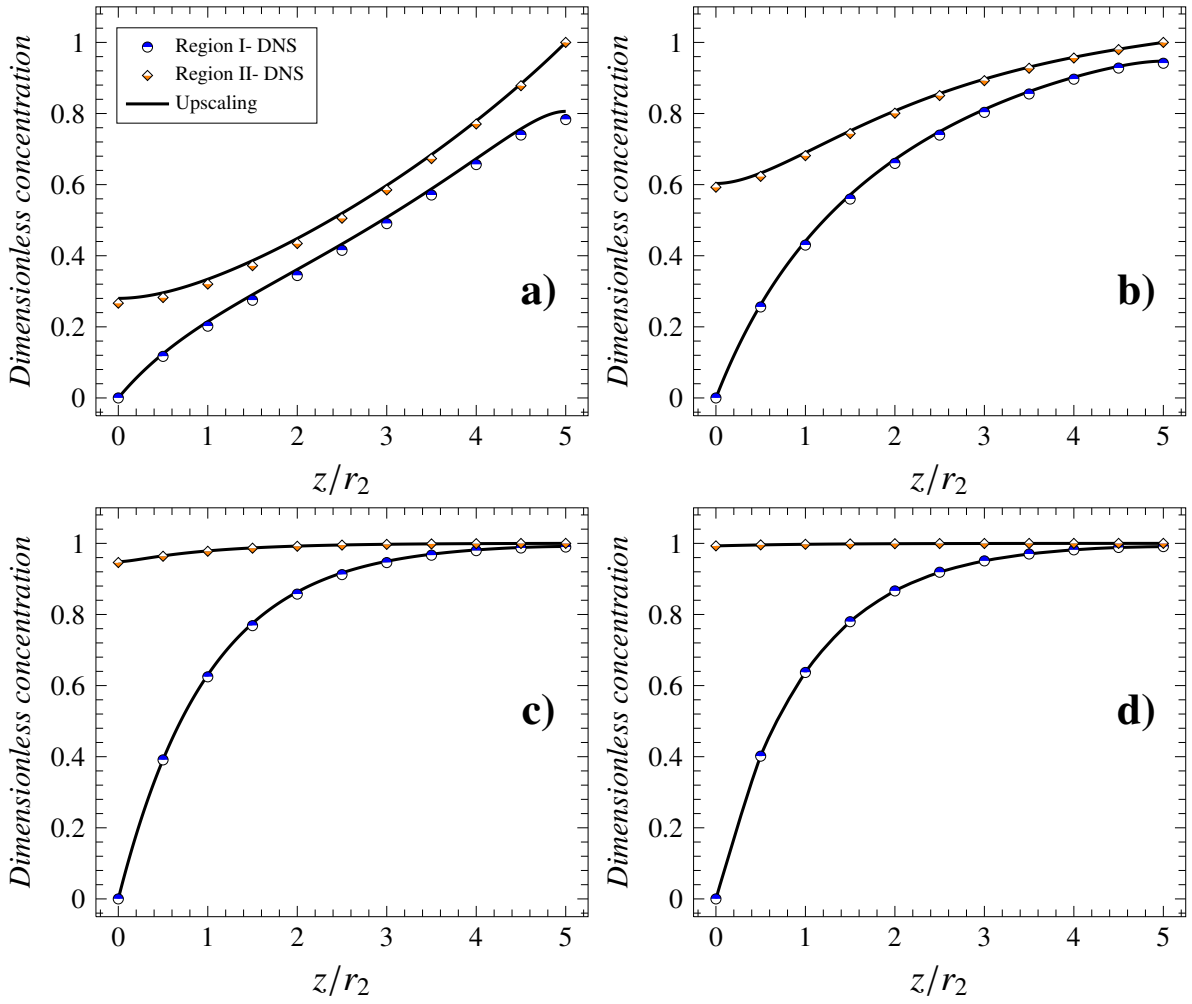

Fig. 8. Dimensionless average concentration profiles obtained with direct numerical simulations (DNS) and upscaling for a) $Pe^{II} = 0.1$, b) $Pe^{II} = 1$, c) $Pe^{II} = 10$ and d) $Pe^{II} = 100$, taking $\xi_1 = 0.5$, $L = 5r_2$, $\mathscr{D}_{AI}/\mathscr{D}_{AII} = 0.5$, $Sh = 1$ and $Pe^{I} = 1$.

Although good agreement (*i.e.*, the relative error percent between the DNS and upscaling is less than 10%) is found in all the comparisons, we note that the largest deviations are found at the exit of Region-II when taking $Sh = 10$. Since this difference appears mainly near the boundary, it leads us to think that the differences arise from the boundary conditions and, in specific, from the location of the dividing surface as suggested by Chandesris and Jamet (2007). This effect is to be expected to be reduced for situations in which $L \gg r_2$.

- In Fig. 7, we present the results of changing the Péclet number in Region-I in three orders of magnitude ranging from 0.1 to 100. Since this dimensionless number relates the rate of convection to the rate of diffusion in Region-I, it follows that if $Pe^{I} < 1$ (Fig. 7a), the residence time of oxygen in the system is increased. Hence, for values of Pe^{I} larger than 1, the permeator exhibits a poor performance. We note also that for $Pe^{I} < 10$, there is good agreement between the concentration profiles predictions resulting from upscaling and DNS. However, as shown in Fig. 7d, we observe that for $Pe^{I} = 100$ there is a clear difference in the predictions. This result is to be expected because $Pe^{I} r_1/L = 10$, violating the first inequality in (21) that

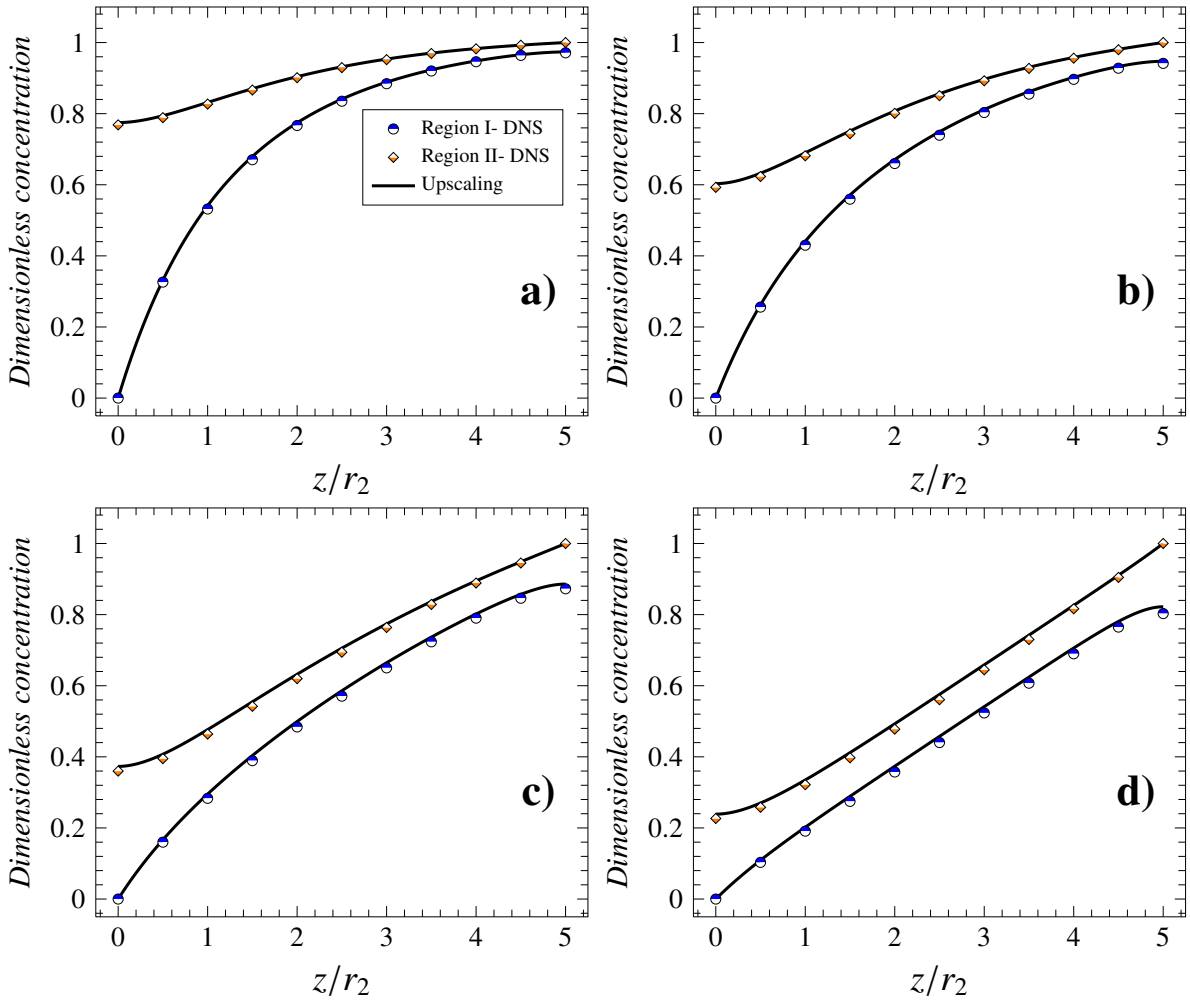

Fig. 9. Dimensionless average concentration profiles obtained with direct numerical simulations (DNS) and upscaling for a) $\mathscr{D}_{AI}/\mathscr{D}_{AII} = 0.25$, b) $\mathscr{D}_{AI}/\mathscr{D}_{AII} = 0.5$, c) $\mathscr{D}_{AI}/\mathscr{D}_{AII} = 1$ and d) $\mathscr{D}_{AI}/\mathscr{D}_{AII} = 1.5$, taking $\xi_1 = 0.5$, $L = 5r_2$, $Sh = 1$ and $Pe^I = Pe^{II} = 1$.

was imposed in the derivation of the closure problem.

- In Fig. 8, we perform a similar analysis to the one performed in Fig. 7, but this time in terms of the Péclet number associated to Region-II. In this case, since oxygen is fed in Region-II, an increment in the convection rate translates into more oxygen available to be transported into Region-I. Notice that, as Pe^{II} increases, the concentration profiles in Region-II tend to the unity (see figs. 8c and 8d). For this reason, we do not observe a plausible difference between the DNS and the upscaled predictions, even for $Pe^{II} = 100$ (Fig. 8d), which does not satisfy the second inequality in (21).

- Finally, in Fig. 9 we present the functionality of the concentration profiles with the ratio of molecular diffusivities $\mathscr{D}_{AI}/\mathscr{D}_{AII}$. We observe that, if $\mathscr{D}_{AII} > \mathscr{D}_{AI}$, the separation process is favored (See Fig. 9a) since the outlet of the noble-gas stream tends to the unity. Interestingly, as the ratio $\mathscr{D}_{AI}/\mathscr{D}_{AII}$ increases, the oxygen concentration in the outlet of the annular section (*i.e.*, the air stream) decreases

while the corresponding values at the outlet of the tube are practically unaffected. In all the computations we observed a close agreement of the predictions resulting from upscaling and DNS.

Conclusions

In this work we derived an upscaled model for studying oxygen separation from an air current, in a shell and tube permeator involving a porous zeolite membrane, to a noble gas current. The model was derived by taking the cross-sectional average in the tube (Region-I) and shell (Region-II) compartments of the equipment and following the steps involved in the method of volume averaging (Whitaker, 1999). The model consists in a set of coupled ordinary differential equations that are written in terms of effective-medium coefficients, which were analytically computed from the solution of the corresponding closure problems. Our analysis showed that the model is sensitive to the following dimensionless parameters: a modified Sherwood number, the Péclet numbers associated to each region and the ratio of molecular diffusivities $\mathscr{D}_{A_I}/\mathscr{D}_{AII}$. The model applicability is bounded by the length-scale constraints given in (21). Hence, as long as these constraints are met, the predictions from the upscaled model are reliable as evidenced from our comparison with direct numerical simulations.

Certainly, since we have the capability of solving the microscale model, it is reasonable to question the need for deriving upscaled models. Albeit the actual computational capabilities allow solving this type of problems, the number of computational nodes needed (after refinement) to obtain a reliable solution of the microscale model can be on the order of millions, whereas for the solution of the upscaled model, this number reduces in three orders of magnitude. Furthermore, the fact that the upscaled model is written in terms of effective medium coefficients allow studying many features from the transport process, just by analyzing the dependence of these coefficients with the relevant variables and parameters of the system. Moreover, in practice, the interest is usually directed to average quantities to evaluate the performance of the system.

As a final point of discussion, we find it convenient to stress the need for a nonequilibrium upscaled model in this particular application. To address this issue, we examine the assumptions and consequences related to an equilibrium model. As explained above, the cross-sectional averaged concentration, $\langle c_A\rangle$ can be expressed in terms of the averaged concentration of each region according to

$$\langle c_A\rangle = \varepsilon\langle c_{AI}\rangle^I + (1-\varepsilon)\langle c_{AII}\rangle^{II} \tag{35}$$

here $\varepsilon = r_1^2/r_2^2$. Under local mass equilibrium conditions, one may assume that (Whitaker, 1999) $(\langle c_{AI}\rangle^I - \langle c_{AII}\rangle^{II})/\langle c_A\rangle \ll 1$ and it follows that

$$\langle c_{AI}\rangle^I \approx \langle c_A\rangle; \quad \langle c_{AII}\rangle^{II} \approx \langle c_A\rangle \tag{36}$$

which implies that the concentration at the shell and tube compartments can be reasonably approximated by a single concentration value. Under these conditions, one may make the substitutions shown in Eq. (36) in eqs. (27) and add the resulting expressions to obtain,

$$v\frac{d\langle c_A\rangle}{dz} = D\frac{d^2\langle c_A\rangle}{dz^2} \tag{37}$$

in which, $v = v_{I,I} - v_{I,II} - v_{II,I} - v_{II,II}$ and $D = D_{I,I} - D_{I,II} - D_{II,I} + D_{II,II}$. This expression is clearly simpler to solve than eqs. (27); however, the price to be paid for this simplification is the lost of information from the interaction with the porous membrane, which is crucial in this process. Furthermore, in practice, it is reasonable to think that experimental measurements are taken at the inlets and outlets of the tube and shell compartments and not at the whole cross section of the system.

From the above, we conclude that the derivation of the upscaled non-equilibrium model provided here is relevant to permeators designed for the separation of oxygen through a noble gas current. In fact, in our research group we are currently performing experiments in a permeator analogous to the one studied in this paper and in a future work we will present the comparison of the resulting experimental measurements with the predictions from the upscaled model.

Acknowledgments

FVP expresses his gratitude to Fondo Sectorial de Investigación para la educación from CONACyT (Project number: 12511908; Arrangement number: 112087) for the financial aid provided. MGH is thankful to PROMEP for the scholarship provided.

Nomenclature

A_i cross-sectional surface of Region-i ($i = I, II$), m^2
$b_{i,j}$ closure variable that maps $d\langle c_{Aj}\rangle^j/dz$ onto $\tilde{c}_{Ai}$ ($i, j = I, II$), m
c_{Ai} concentration of species A in Region-i ($i = I, II$), mol/m^3
$\tilde{c}_{Ai}$ concentration deviations of species A in Region-i ($i = I, II$), mol/m^3
$\langle c_A\rangle$ cross-sectional average of the concentration of species A, mol/m^3
$\langle c_{Ai}\rangle^i$ cross-sectional average of the concentration of species A in Region-i ($i = I, II$), mol/m^3
D dispersion coefficient in the equilibrium model, m^2/s
$D_{i,j}$ dispersion coefficients in the non-equilibrium model, ($i, j = I, II$), m^2/s
$\mathscr{D}_{Ai}$ molecular diffusivity of species A in Region-i ($i = I, II$), m^2/ s
D_{eff} effective diffusivity in the porous membrane, m^2/ s
g gravity, m^2/s
$h^{I,II}$ inter-regional transport coefficient in the upscaled model, m^2/ s
ℓ width of the membrane, m
L length of the system, m
p_i pressure in Region-i ($i = I, II$), Pa
P permeability of the porous membrane, m/s
Pe^i Péclet number associated to Region-i ($i = I, II$)
r radial direction, m
s_i closure variable that maps $\left(\langle c_{AI}\rangle^I - \langle c_{AII}\rangle^{II}\right)$ onto $\tilde{c}_{Ai}$, ($i = I, II$)
Sh modified Sherwood number
r_1, r_2 radius of regions I and II, respectively, m
v velocity coefficient in the equilibrium model, m/s
$v_{i,j}$ velocity coefficients in the non-equilibrium model ($i, j = I, II$), m/s
v_{zi} velocity field in Region-i ($i = I, II$), m/s
$\tilde{v}_{zi}$ velocity deviations in Region-i ($i = I, II$), m/s
z axial direction, m
Z dimensionless axial direction

Greek symbols

μ_i viscosity of the fluid in Region i ($i = I, II$), kg/ms
θ angular direction, rad
ρ_i density of the fluid in Region i ($i = I, II$), kg/m^3

Subscripts

$i0$ value of a property at $z = 0$ in Region i ($i = I, II$)
iL value of a property at $z = L$ in Region i ($i = I, II$)

References

Abdel-Jawad M.M., Gopalakrishnan S., Duke M.C., Macrossan M.N., Smith Schneider P., Diniz da Costa J.C. (2007). Flow fields on feed and permeate sides of tubular molecular sieving silica (MSS) membranes. *Journal of Membrane Science 299*, 229-235.

Bowen T.C., Noble R.D., Falconer J.L. (2004). Fundamentals and applications of pervaporation through zeolite membranes. *Journal of Membrane Science 245*, 1-33.

Bird R.B., Stewart W.E., Lightfoot E.N. (2007). *Transport Phenomena*, second edition, Wiley.

Chandesris M. and Jamet D. (2007). Boundary conditions at a fluid-porous interface: An *a priori* estimation of the stress jump coefficients. *International Journal of Heat and Mass Transfer 50*, 3422-3436.

Coronas J., Santamaría J. (1999). Catalytic reactors based on porous ceramic membranes. *Catalysis Today 51*, 377-389.

Cushman J. (1997). *The Physics of Fluids in Hierarchical Porous Media: Angstroms to Miles*, Springer.

Faucheux V., Audier M., Rapenne L., Pignard S. (2008). Fabrication of thin and dense nano-crystalline membranes on porous substrates. *Journal of Materials Processing Technology 204*, 248-254.

Freeman B., Yampolskii Y., Pinnau I. (2008). *Materials Science of Membranes for Gas and Vapor Separation*, Wiley.

Gascon J., Kapteijn F., Zornoza B., Sebastián V., Casado C., Coronas J. (2012). Practical approach to zeolitic membranes and coatings: State of the art, opportunities, barriers, and future perspectives. *Chemistry of Materials 24*, 2829-2844.

Gray W.G. (1975). A derivation of the equations for multiphase transport. *Chemical Engineering Science 30*, 229-233.

Hernández M.G., Salinas-Rodríguez E., Gómez S., Roa-Neri J.A.E., Rodríguez R.F. (2012). Membranas zeolíticas y sus principales aplicaciones. *Materiales Avanzados 18*, 9-18.

Hussain A., Seidel-Morgenstern A., Tsotsas E. (2006). Heat and mass transfer in tubular ceramic membranes for membrane reactors. *International Journal of Heat and Mass Transfer 49*, 2239-2253.

Jiang Q., Faraji S., Slade D.A., Stagg-Williams S.M. (2011). Chapter 11 - A Review of Mixed Ionic and Electronic Conducting Ceramic Membranes as Oxygen Sources for High-Temperature Reactors, In: S. Ted Oyama and Susan M. Stagg-Williams, Editor(s), *Membrane Science and Technology*, Elsevier, Volume 14, Pages 235-273.

Kumar V.S., Hariharan K.S., Mayya K.S., Han S. (2013). Volume averaged reduced order Donnan Steric Pore Model for nanofiltration membranes. *Desalination 322*, 21-28.

Li S., Jin W., Huang P., Xu N., Shi J., Lin Y.S. (2000). Tubular lanthanum cobaltite perovskite type membrane for oxygen permeation. *Journal of Membrane Science 166*, 51-61.

Liang F., Jiang H., Schiestel T., Caro J. (2010). High-purity oxygen production from air using Perovskite hollow fiber membranes. *Industrial and Engineering Chemistry Research 49*, 9377-9384.

McLeary E.E., Jansen J.C., Kapteijn F. (2006). Zeolite based films, membranes and membrane reactors: Progress and prospects. *Microporous and Mesoporous Materials 90*, 198-220.

Rebollar-Perez G., Carretier E., Moulin P. (2010). Aplicaciones de la permeación de vapor: El tratamiento de compuestos orgánicos volátiles de origen antropogénico. *Revista Mexicana de Ingeniería Química 9*, 67-77.

Taylor G.I. (1953). Dispersion of soluble matter in solvent flowing slowly through a tube. *Proceedings of the Royal Society of London Series A, Mathematical and Physical Sciences 219*, 186-203.

Taylor G.I. (1954). Conditions under which dispersion of a solute in a stream of solvent can be used to measure molecular diffusion. *Proceedings of the Royal Society of London Series A, Mathematical and Physical Sciences 225*, 473-477.

Wang H., Cong Y., Yang W. (2003). Investigation on the partial oxidation of methane to syngas in a tubular $Ba_{0.5}Sr_{0.5}Co_{0.8}Fe_{0.2}O_3 - \delta$ membrane reactor. *Catalysis Today 82*, 157-166.

Wang H., Wang R., Tee Liang D., Yang W. (2004). Experimental and modeling studies on $Ba_{0.5}Sr_{0.5}Co_{0.8}Fe_{0.2}O_3 - \delta$ (BSCF) tubular membranes for air separation. *Journal of Membrane Science 243*, 405-415.

Whitaker S. (1999). *The Method of Volume Averaging*, Kluwer academic publishers.

Whitaker S. (2009). Chemical engineering education: making connections at interfaces. *Revista Mexicana de Ingeniería Química 8*, 1-33.

Wood B.D. (2009). Taylor-Aris dispersion: An explicit example for understanding multiscale analysis via volume averaging. *Chemical Engineering Education 43*, 29-38.

Wood B.D., Valdés-Parada F.J. (2013). Volume averaging: Local and nonlocal closures using a Green's function approach. *Advances in Water Resources 51*, 139-167.

Zhu X., Sun S., He Y., Cong Y., Yang W. (2008). New concept on air separation. *Journal of Membrane Science 323*, 221-224.

Appendix A: Closure problem statement for mass transfer

In this section we derive and solve the closure problem for mass transfer in both regions of the system. With this aim, let us subtract Eq. (14a) to Eq. (1a) in order to obtain

$$\underbrace{\langle v_{zI}\rangle^I \frac{\partial \tilde{c}_{AI}}{\partial z}}_{\mathbf{o}\left(\frac{\langle v_{zI}\rangle^I \tilde{c}_{AI}}{L}\right)} + \tilde{v}_{zI}\frac{\partial \langle c_{AI}\rangle^I}{\partial z} + \underbrace{\tilde{v}_{zI}\frac{\partial \tilde{c}_{AI}}{\partial z}}_{\mathbf{o}\left(\frac{\langle v_{zI}\rangle^I \tilde{c}_{AI}}{L}\right)} - \underbrace{\left\langle \tilde{v}_{zI}\frac{\partial \tilde{c}_{AI}}{\partial z}\right\rangle^I}_{\mathbf{o}\left(\frac{\langle v_{zI}\rangle^I \tilde{c}_{AI}}{L}\right)} = \underbrace{\frac{\mathscr{D}_{AI}}{r}\frac{\partial}{\partial r}\left(r\frac{\partial \tilde{c}_{AI}}{\partial r}\right)}_{\mathbf{o}\left(\frac{\mathscr{D}_{AI}\tilde{c}_{AI}}{r_1^2}\right)} + \underbrace{\mathscr{D}_{AI}\frac{\partial^2 \tilde{c}_{AI}}{\partial z^2}}_{\mathbf{o}\left(\frac{\mathscr{D}_{AI}\tilde{c}_{AI}}{L^2}\right)} - \underbrace{\frac{2\mathscr{D}_{AI}}{r_1}\left.\frac{\partial \tilde{c}_{AI}}{\partial r}\right|_{r_1}}_{\mathbf{o}\left(\frac{\mathscr{D}_{AI}\tilde{c}_{AI}}{r_1^2}\right)} \tag{A.1}$$

here we have included the estimates of order of magnitude of each homogeneous term with the aim of pondering about the relevance that each of them play in Eq. (A.1). Notice that, for the dispersive terms, we have taken into account Eq. (19a) that leads us to conclude that $\tilde{v}_{zI} = \mathbf{O}(\langle v_{zI}\rangle^I)$. From these estimates we notice that the diffusive term in the radial direction overcomes its counterpart in the axial direction, *i.e.*,

$$\mathscr{D}_{AI}\frac{\partial^2 \tilde{c}_{AI}}{\partial z^2} \ll \frac{\mathscr{D}_{AI}}{r}\frac{\partial}{\partial r}\left(r\frac{\partial \tilde{c}_{AI}}{\partial r}\right) \tag{A.2}$$

as long as the following length-scale constraint is met

$$r_1^2 \ll L^2 \tag{A.3}$$

Furthermore, all the convective terms may also be neglected with respect to the diffusive term in the radial direction,

$$\langle v_{zI}\rangle^I \frac{\partial \tilde{c}_{AI}}{\partial z},\ \tilde{v}_{zI}\frac{\partial \tilde{c}_{AI}}{\partial z},\ \left\langle \tilde{v}_{zI}\frac{\partial \tilde{c}_{AI}}{\partial z}\right\rangle^I \ll \frac{\mathscr{D}_{AI}}{r}\frac{\partial}{\partial r}\left(r\frac{\partial \tilde{c}_{AI}}{\partial r}\right) \tag{A.4}$$

on the basis of the length-scale constraint

$$\underbrace{\frac{\langle v_{zI}\rangle^I r_1}{\mathscr{D}_{AI}}}_{Pe^I}\frac{r_1}{L} \ll 1 \tag{A.5}$$

Notice that this last constraint is consistent with the one originally proposed by Taylor (1953, 1954) where we have identified a Péclet number definition that will be relevant in the evaluation of the model. Under these circumstances, Eq. (A.1) is dramatically reduced to

$$\underbrace{\tilde{v}_{zI}\frac{d\langle c_{AI}\rangle^I}{dz}}_{volume\ source} = \frac{\mathscr{D}_{AI}}{r}\frac{\partial}{\partial r}\left(r\frac{\partial \tilde{c}_{AI}}{\partial r}\right) - \frac{2\mathscr{D}_{AI}}{r_1}\left.\frac{\partial \tilde{c}_{AI}}{\partial r}\right|_{r_1} \tag{A.6}$$

here we have regarded the non-homogeneous term in the differential equation as a volumetric source. It is worth noting that, due to the constraint in (A.5), for the determination of the concentration deviation fields, $d\langle c_{AI}\rangle^I/dz$ can be safely regarded as a constant. Following the same procedure for *Region-II*, we have that the concentration deviations solve the differential equation

$$\underbrace{-\tilde{v}_{zII}\frac{d\langle c_{AII}\rangle^{II}}{dz}}_{volume\ source} = \frac{\mathscr{D}_{AII}}{r}\frac{\partial}{\partial r}\left(r\frac{\partial \tilde{c}_{AII}}{\partial r}\right) + \frac{2\mathscr{D}_{AII}r_1}{(r_2^2 - r_1^2)}\left.\frac{\partial \tilde{c}_{AII}}{\partial r}\right|_{r_1} \tag{A.7}$$

The length-scale constraints supporting this result are,

$$\underbrace{\frac{\langle v_{zII}\rangle^{II} r_2}{\mathscr{D}_{AII}}}_{Pe^{II}}\frac{r_2}{L} \ll 1 \tag{A.8a}$$

$$r_2^2 \ll L^2 \tag{A.8b}$$

To determine the boundary conditions applying to the concentration deviations, let us substitute the spatial decomposition $c_{Ai} = \langle c_{Ai}\rangle^i + \tilde{c}_{Ai}$ $(i = I, II)$ into eqs. (3c), (3d) and (3f); the resulting expressions are

$$at\ \ r = r_1, \quad \mathscr{D}_{AI}\frac{\partial \tilde{c}_{AI}}{\partial r} = \mathscr{D}_{AII}\frac{\partial \tilde{c}_{AII}}{\partial r} \tag{A.9a}$$

$$at\ \ r = r_1, \quad -\mathscr{D}_{AI}\frac{\partial \tilde{c}_{AI}}{\partial r} = P(\tilde{c}_{AI} - \tilde{c}_{AII}) + \underbrace{P(\langle c_{AI}\rangle^I - \langle c_{AII}\rangle^{II})}_{surface\ \ source} \tag{A.9b}$$

$$at\ \ r = r_2, \quad \mathscr{D}_{AII}\frac{\partial \tilde{c}_{AII}}{\partial r} = 0 \tag{A.9c}$$

Finally, the concentration deviations fields must be defined for all values of r and must also satisfy the average constraints

$$\langle \tilde{c}_{AI}\rangle^I = 0; \quad \langle \tilde{c}_{AII}\rangle^{II} = 0 \tag{A.10}$$

It is worth emphasizing the linear nature of the closure problem, which is driven by the volume sources $d\langle c_{AI}\rangle^I/dz$ and $d\langle c_{AII}\rangle^{II}/dz$ as well as by the surface source $(\langle c_{AI}\rangle^I - \langle c_{AII}\rangle^{II})$. These features will be exploited in the derivation of the closure problem solution.

Appendix B: Closure problem solution

This section is devoted to the derivation of the analytical solution of the closure problem. To achieve this goal, we integrate Eq. (A.6) twice taking into account the fact that the deviation fields must be

defined for any value of r, the resulting expression can be written as

$$\tilde{c}_{AI} = \frac{Pe^I}{4\xi_1}\left(\xi^2 - \frac{\xi^4}{2\xi_1^2}\right)\frac{d\langle c_{AI}\rangle^I}{dZ} + \frac{\xi^2}{2\xi_1}\left.\frac{\partial\tilde{c}_{AI}}{\partial\xi}\right|_{\xi_1} + c_I \tag{B.1}$$

here $Z = z/r_2$.

Furthermore, integrating twice Eq. (A.7), taking into account the Neumann-type boundary condition in Eq. (A.9c) as well as the boundary condition in Eq. (A.9a), leads to

$$\tilde{c}_{AII} = \frac{Pe^{II}}{2\delta}\left[\xi^2\ln\frac{\xi}{\xi_1} - \frac{\xi^2}{2} - \left(\frac{\left(\xi_1^2-1\right)\xi^2}{2} - \frac{\xi^4}{4} + \xi_1^2\ln\xi\right)\chi\right]\frac{d\langle c_{AII}\rangle^{II}}{dZ} + \frac{\xi_1\mathscr{D}_{AI}}{\left(1-\xi_1^2\right)\mathscr{D}_{AII}}\left.\frac{\partial\tilde{c}_{AI}}{\partial\xi}\right|_{\xi_1}\left(\ln\xi - \frac{\xi^2}{2}\right) + c_{II} \tag{B.2}$$

To determine the constants of integration c_I and c_{II} we use the average constraints given in Eq. (A.10), in order to obtain,

$$c_I = -\frac{Pe^I\xi_1}{12}\frac{d\langle c_{AI}\rangle^I}{dZ} - \frac{\xi_1}{4}\left.\frac{\partial\tilde{c}_{AI}}{\partial\xi}\right|_{\xi_1} \tag{B.3a}$$

$$c_{II} = -\frac{Pe^{II}}{\delta}\frac{d\langle c_{AII}\rangle^{II}}{dZ}\left[-\left(\frac{1}{4}\chi + \frac{3\left(1+\xi_1^2\right)}{16}\right) + \left(4 + 3\xi_1^2 - 9\xi_1^4 + 2\xi_1^6 + 12\xi_1^4\ln\xi_1\right)\frac{\chi}{24\left(1-\xi_1^2\right)}\right] + \frac{\xi_1\mathscr{D}_{AI}}{\left(1-\xi_1^2\right)\mathscr{D}_{AII}}\left.\frac{\partial\tilde{c}_{AI}}{\partial\xi}\right|_{\xi_1}\left(\xi_1^2\chi + \frac{3+\xi_1^2}{4}\right) \tag{B.3b}$$

Clearly the fields of the closure variables, in their present form, are written in terms of $\left.\frac{\partial\tilde{c}_{AI}}{\partial\xi}\right|_{\xi_1}$, which is unknown. To determine it, we make use of the boundary condition given by Eq. (A.9b); the resulting expression is

$$\xi_1\left.\frac{\partial\tilde{c}_{AI}}{\partial\xi}\right|_{\xi_1} = Pe^I\xi_1\alpha\frac{d\langle c_{AI}\rangle^I}{dZ} \pm Pe^{II}\beta\frac{d\langle c_{AII}\rangle^{II}}{dZ} + 24\alpha\left(\langle c_{AI}\rangle^I - \langle c_{AII}\rangle^{II}\right) \tag{B.4}$$

As a matter of brevity, we introduced the following definitions,

$$Sh = \frac{\mathrm{P}\,r_2}{\mathscr{D}_{AI}} \tag{B.5a}$$

$$\alpha = \left[\frac{\mathscr{D}_{AI}}{\mathscr{D}_{AII}}\left(\frac{24\chi + 6\left(3-\xi_1^2\right)}{1-\xi_1^2}\right) - 6 - \frac{24}{Sh\xi_1}\right]^{-1} \tag{B.5b}$$

$$\beta = \frac{\alpha}{\delta}\left[\left(\xi_1^6 - 3\xi_1^2 + 2 - 12\xi_1^2\ln\xi_1\right)\frac{\chi}{\left(1-\xi_1^2\right)} - \frac{3}{2}\left(\xi_1^2 - 3\right)\right] \tag{B.5c}$$

In this way, we may re-write eqs. (B.1) and (B.2) in their final form,

$$\tilde{c}_{AI} = \frac{Pe^I\xi_1}{4}\left(\frac{(2\alpha+1)\xi^2}{\xi_1^2} - \frac{\xi^4}{2\xi_1^4} - \frac{1}{3} - \alpha\right)\frac{d\langle c_{AI}\rangle^I}{dZ} - Pe^{II}\frac{\beta}{2}\left(\frac{\xi^2}{\xi_1^2} - \frac{1}{2}\right)\frac{d\langle c_{AII}\rangle^{II}}{dZ} + 12\alpha\left(\frac{\xi^2}{\xi_1^2} - \frac{1}{2}\right)\left(\langle c_{AI}\rangle^I - \langle c_{AII}\rangle^{II}\right) \tag{B.6a}$$

$$\tilde{c}_{AII} = Pe^I\frac{\xi_1\mathscr{D}_{AI}\alpha}{\left(1-\xi_1^2\right)\mathscr{D}_{AII}}\left(\ln\xi - \frac{\xi^2}{2} + \xi_1^2\chi + \frac{3+\xi_1^2}{4}\right)\frac{d\langle c_{AI}\rangle^I}{dZ} - \frac{Pe^{II}}{\delta}\left[-\frac{1}{2}\xi^2\ln\frac{\xi}{\xi_1} - \frac{\xi^4\chi}{8} + \frac{\gamma_1\xi^2/4 + \gamma_2\ln\xi + \gamma_0}{1-\xi_1^2}\right]\frac{d\langle c_{AII}\rangle^{II}}{dZ} + \frac{24\mathscr{D}_{AI}\alpha}{\left(1-\xi_1^2\right)\mathscr{D}_{AII}}\left(\ln\xi - \frac{\xi^2}{2} + \xi_1^2\chi + \frac{3+\xi_1^2}{4}\right)\left(\langle c_{AI}\rangle^I - \langle c_{AII}\rangle^{II}\right) \tag{B.6b}$$

which have the same structure as eqs. (22). To simplify the structure of eqs. (B.6), we introduced

$$\gamma_0 = \frac{\mathscr{D}_{AI}\delta\beta}{\mathscr{D}_{AII}}\left(\xi_1^2\chi\ln\xi_1 + \frac{3+\xi_1^2}{4}\right) - \frac{1}{4}\left(\ln\xi_1 + \frac{3\left(1-\xi_1^4\right)}{4}\right) + \left(4 + 3\xi_1^2 - 9\xi_1^4 + 2\xi_1^6 + 12\xi_1^4\ln\xi_1\right)\frac{\chi}{24} \tag{B.7a}$$

$$\gamma_1 = \left(\xi_1^2 - 1\right)(\ln\xi_1 - 1) - \frac{2\mathscr{D}_{AI}\delta\beta}{\mathscr{D}_{AII}} \tag{B.7b}$$

$$\gamma_2 = \frac{\ln\xi_1}{2}\xi_1^2 + \frac{\mathscr{D}_{AI}\delta\beta}{\mathscr{D}_{AII}} \tag{B.7c}$$